NG2 glia protect against prion neurotoxicity by inhibiting prostaglandin E2 signaling

Yingjun Liu[1, *], Jingjing Guo[1], Maja Matoga[1], Marina Korotkova[2], Per-Johan Jakobsson[2], Adriano Aguzzi[1, *]

[1] Institute of Neuropathology, University of Zurich, Switzerland

[2] Department of Medicine, Karolinska Institutet, Sweden

[*] Correspondence

Adriano Aguzzi or Yingjun Liu:

Institute of Neuropathology, University of Zurich,

Schmelzbergstrasse 12, 8091 Zurich, Switzerland.

Telephone: +41 44 255 21 07.

Email: adriano.aguzzi@usz.ch or yingjun.liu@bsse.ethz.ch

Abstract

Oligodendrocyte-lineage cells, including NG2 glia, undergo prominent changes in various neurodegenerative disorders. This raises the question of how myelinating cells interact with neurodegenerative processes. Here, we found that NG2 glia were activated after prion infection in cerebellar organotypic cultured slices (COCS) and in brains of prion-inoculated mice. In both model systems, depletion of NG2 glia exacerbated prion-induced neurodegeneration and accelerated prion pathology. Loss of NG2 glia unleashed a microglial reaction promoting the biosynthesis of prostaglandin E2 (PGE2), which augmented prion neurotoxicity in the HovS cell line, primary neurons and COCS through binding to the EP4 receptor. Single-cell RNA sequencing revealed molecular signatures of inflammatory, disease-associated and MHC^+ microglia but not of interferon-responsiveness in PGE2-producing microglia of prion-inoculated mice. Pharmacological or genetic inhibition of PGE2 biosynthesis attenuated prion-induced neurodegeneration in COCS and mice, reduced the enhanced neurodegeneration in NG2-glia-depleted COCS after prion infection, and dampened the acceleration of prion disease in NG2-glia-depleted mice. These data unveil a non-cell-autonomous interaction between NG2 glia and microglia in prion disease and suggest that PGE2 signaling may represent an actionable target against prion diseases.

Introduction

Neurodegenerative diseases such as Alzheimer's disease (AD), Parkinson's disease (PD) and prion diseases involve multiple cell types and various genetic and environmental factors (Wareham, Liddelow et al. 2022). Accumulating evidence suggest that both cell-autonomous and non-cell-autonomous mechanisms contribute to the neurodegenerative process (Aguzzi and Liu 2017, Liu and Aguzzi 2019). Among the common neurodegenerative disorders, prion diseases can be best mimicked with laboratory animal models (Brandner and Jaunmuktane 2017). Prion-inoculated mice develop a fatal neurodegenerative condition that is almost indistinguishable from its human counterpart at the neuropathological level, providing an invaluable model system for investigating the cellular and molecular mechanisms of chronic neurodegeneration relevant to humans.

Different neurodegenerative diseases have distinct initial pathogenic triggers and clinical manifestations, yet certain molecular and cellular alterations, such as abnormal protein aggregation and activation of glial cells, are common to all these disorders (Wareham, Liddelow et al. 2022). Large amounts of data support vital roles of microglia and astrocytes in the initiation and progression of neurodegeneration. However, the function of other cell types, including oligodendrocyte-lineage cells, in the pathogenesis of neurodegenerative diseases has been elusive, and investigations on this crucial aspect were largely ignored by the neurodegenerative disease community. Recent advances in high resolution gene expression analyses have enabled a deeper understanding of this complex cellular landscape. In addition to confirming the alterations of microglia and astrocytes, single-cell and spatial transcriptomics analyses of brain tissues from patients and animal models have unraveled prominent changes of oligodendrocyte linage cells in multiple neurodegenerative disorders (Mathys, Davila-Velderrain et al. 2019, Chen, Lu et al. 2020, Pandey, Shen et al. 2022), including prion diseases (Dimitriadis, Zhang et al. 2022, Slota, Sajesh et al. 2022).

Oligodendrocyte-lineage cells are traditionally considered as supportive cells in the central nervous system (CNS), producing myelin sheaths that insulate nerve fibers and help speed up transmission of electrical signals along neuronal axons. It is unclear how myelinating cells interact with other cell types of the brain in the context of neurodegenerative process. Here we investigated the role of oligodendrocyte precursor cells (NG2 glia) in chronic neurodegeneration induced by prion infections. We found that NG2 glia were neuroprotective and played a crucial role in influencing the microglial pathway that is responsible for the biosynthesis of prostaglandin E2 (PGE2), which promotes prion-induced neurodegeneration through binding to the EP4 receptor. These data suggest that NG2 glia have an impact on an intricate cell-cell interaction network in prion disease, and highlight NG2 glia and PGE2 signaling as potential targets for disease-modifying therapies against neurodegenerative disorders.

68 **Results**

69 *NG2 glia activation in prion disease models*

70 Our previous gene expression analyses of prion-inoculated mice (Sorce, Nuvolone et al. 2020)
71 and prion-infected cerebellar organotypic cultured slices (COCS) (Liu, Senatore et al. 2022),
72 as well as recent single-cell transcriptomics from other groups (Dimitriadis, Zhang et al. 2022,
73 Slota, Sajesh et al. 2022), point to possible transcriptional changes in NG2 glia during prion
74 disease. However, it is unclear how these cells respond to prion infections at the cellular level.
75 We therefore examined the markers of NG2 glia, including NG2 and platelet-derived growth
76 factor receptor alpha (Pdgfrα), in prion-infected COCS and mouse brains by western blotting
77 and immunofluorescence. We found an increase in NG2 protein levels in both paradigms (**Fig.**
78 **1a-d**). The protein level of Pdgfrα was also upregulated in mouse brains after prion infection,
79 although not as much as NG2 (**Fig. 1c-d**). Similarly, we observed enhanced NG2 immunore-
80 activity in prion-infected C57BL/6J and Tga20 COCS as well as in prion-inoculated mouse
81 brains (**Fig. 1e-h** and **Supplementary Fig. 1a-b**). After prion infection, NG2 glia exhibited
82 enlargement of cell bodies and arborization of cellular processes (**Fig. 1g**), reminiscent of the
83 NG2 glia phenotypes in mouse models of brain injuries (Alonso 2005, Jin, Riew et al. 2018),
84 suggesting that neuronal damage plays a role in prion-induced NG2 glia activation.

85

86 *Loss of NG2 glia enhances prion neurotoxicity and accelerates prion disease*

87 To facilitate functional investigations of NG2 glia, we previously developed efficient and selec-
88 tive NG2 glia depletion strategies ex vivo and in vivo (Liu and Aguzzi 2020). We used the
89 PDGFR inhibitor CP673451 to deplete NG2 glia from COCS, and combined cell-type selective
90 diphtheria toxin receptor (DTR) expression with systemic DT injections for in vivo NG2 glia
91 depletion (Liu and Aguzzi 2020).

92 To determine the functional relevance of NG2 glia in prion-induced neurodegeneration, we
93 depleted NG2 glia from COCS by continuous (**Supplementary Fig. 2a-b**) or transient (**Sup-**
94 **plementary Fig. 3a**) CP673451 treatment in the presence or absence of prions, and com-
95 pared them to DMSO-treated controls. Again, we saw enhanced NG2 immunoreactivity in
96 prion-infected C57BL/6J and Tga20 COCS and – as expected – NG2 glia loss in both unin-
97 fected and prion-infected COCS after continuous CP673451 treatment (**Fig. 2a-b** and **Sup-**
98 **plementary Fig. 2c-d**). Although NG2 glia depletion did not influence neuronal survival in the
99 absence of prions, it enhanced neurodegeneration in prion-exposed C57BL/6J and Tga20
100 COCS (**Fig. 2a-b** and **Supplementary Fig. 2c-d**), suggesting a neuroprotective role of NG2
101 glia under pathological conditions. A similar enhancement of neurodegeneration was also ob-
102 served in prion-infected COCS after transient CP673451 treatment (**Supplementary Fig. 3b-**
103 **c**). Interestingly, NG2 glia number was largely restored 3 weeks after transient CP673451

treatment in prion-infected COCS (**Supplementary Fig. 3b-c**), suggesting that short-term destruction of NG2 glia suffices to influence prion neurotoxicity.

To investigate the effects of NG2 glia depletion on prion disease in vivo, we crossed Pdgfrα-CreER mice with iDTR mice and generated Pdgfrα-CreER/iDTR (Pdgfrα^{iDTR}) mice. Pdgfrα-CreER and iDTR littermates were used for controls. We inoculated mice with prions one month after tamoxifen treatment, and administered DT daily for 5 days at 12 or 16-weeks post inoculation (wpi) (**Supplementary fig. 4a**). According to immunofluorescent examinations, there was ~50% decrease of NG2 glia number in the brains of Pdgfrα^{iDTR} mice compared to controls after DT injection (Liu and Aguzzi 2020). Prion disease was accelerated in NG2-glia-depleted Pdgfrα^{iDTR} mice of both sexes when NG2 glia depletion was induced at 16 wpi (**Fig. 2c**), and in male mice when NG2 glia depletion was induced at 12 wpi (**Supplementary Fig. 4b**), possibly attributable to the sex effects on the incubation time of prion disease in animal models (Loeuillet, Boelle et al. 2010, Akhtar, Wenborn et al. 2011).

Early neurodegeneration in prion disease is characterized by severe dendritic pathology (Fuhrmann, Mitteregger et al. 2007), which can be best visualized in the hippocampus. To investigate whether loss of NG2 glia affects prion-induced neurodegeneration in vivo, we inoculated a second cohort of Pdgfrα^{iDTR} and control mice after tamoxifen treatment, administered DT at 16 wpi and collected brains 4 weeks thereafter at ~21 wpi. Immunostaining of NG2 confirmed reduction of NG2 glia number in Pdgfrα^{iDTR} mice compared to controls (**Fig. 2d-e**). We then examined hippocampal dendritic pathology by Map2 immunofluorescence. As expected, we observed dendritic damages characterized by dendritic varicosities and fragmentation in both NG2 glia intact and NG2-glia-depleted mice after prion infection (**Fig. 2d**). However, the density of surviving dendrites was less in Pdgfrα^{iDTR} mice than in control mice (**Fig. 2d-e**), suggesting that NG2 glia deficiency also enhances prion-induced neurodegeneration in vivo. HE staining indicated similar spongiform changes in the brains of prion-inoculated Pdgfrα^{iDTR} mice and control mice (**Supplementary Fig. 5**).

Loss of NG2 glia does not influence PrP^{C} expression, prion replication and prion-induced neuroinflammation

PrP^{C} is the substrate of prion replication (Bueler, Aguzzi et al. 1993), and is essential for prion disease pathogenesis (Brandner, Isenmann et al. 1996). Tissue abundance of PrP^{C} correlates with the incubation time of prion disease in animal models (Fischer, Rulicke et al. 1996, Minikel, Zhao et al. 2020). We therefore examined the levels of PrP^{C} and PrP^{Sc} (the protease K-resistant pathological PrP) in NG2-glia-depleted COCS and mice by western blotting. We found that neither the PrP^{C} (**Supplementary Fig. 6a-b**) nor the PrP^{Sc} levels (**Supplementary Fig. 6c-d**) noticeably changed in COCS treated with CP673451 compared to controls. In addition, similar levels of PrP^{C} (**Supplementary Fig. 6e-f**) and PrP^{Sc} (**Supplementary Fig. 6g-**

141 **h**) were observed in the brains of NG2-glia-depleted Pdgfrα^{iDTR} mice and control mice. Hence,
142 enhanced neurodegeneration and accelerated prion disease after NG2 glia depletion were not
143 caused by alterations of PrP^{C} expression and prion replication.
144 We previously found that NG2 glia were required for maintaining the homeostatic microglia
145 state (Liu and Aguzzi 2020). However, depletion of NG2 glia in cultured brain slices and adult
146 mice did not influence microglia numbers or induce notable changes of tissue-level neuroin-
147 flammatory responses under normal conditions (Liu and Aguzzi 2020). To determine whether
148 loss of NG2 glia affects prion-induced microglia activation and neuroinflammation, we com-
149 pared the density of Cd68^{+} reactive microglia between NG2-glia-depleted and intact COCS in
150 the presence or absence of prions. We found that reactive microglia were rare in control
151 COCS, but their number increased after prion infection (**Supplementary Fig. 7a-b**). Never-
152 theless, the levels of microglia activation were comparable between NG2-glia-depleted and
153 intact COCS, with or without prion infection (**Supplementary Fig. 7a-b**). Similarly, we did not
154 observe any changes of Iba1 and Cd68 immunoreactivity in NG2-glia-depleted brains after
155 prion inoculation (**Supplementary Fig. 7c-d**). Furthermore, the mRNA levels of the proinflam-
156 matory factors, tumor necrosis factor alpha (TNFα), Interleukin 1 beta (IL1β) and IL12β, were
157 unaltered by NG2 glia depletion in COCS and mouse brains after prion infection (**Supplemen-**
158 **tary Fig. 8a-b**). Collectively, these data suggest that loss of NG2 glia does not change prion-
159 induced microglia activation and neuroinflammation at tissue level.
160
161 *Loss of NG2 glia enhances the pathway that is responsible for PGE2 biosynthesis*
162 When evaluating gene expression changes in NG2-glia-depleted COCS with RNA sequencing
163 (Liu and Aguzzi 2020), we noticed possible dysregulation of genes related to the biosynthesis
164 of PGE2, which was reported to be increased in the cerebral spinal fluid (CSF) of prion disease
165 patients (Minghetti, Greco et al. 2000, Minghetti, Cardone et al. 2002).
166 To confirm the potential influence of NG2 glia on PGE2, we depleted NG2 glia in COCS with
167 CP673451, and examined the expression levels of cyclooxygenase 2 (Cox2) and prostaglan-
168 din E synthase (Ptges), two major enzymes responsible for PGE2 biosynthesis under patho-
169 logical conditions. Both immunofluorescence and qRT-PCR results confirmed efficient NG2
170 glia depletion after CP673451 treatment (**Fig. 3a-c**). Importantly, we found that the expression
171 levels of both Cox2 and Ptges were upregulated in NG2-glia-depleted COCS compared to
172 NG2 glia intact COCS (**Fig. 3c**). Furthermore, we treated COCS with PDGFAA, the ligand for
173 Pdgfrα, which promotes NG2 glia proliferation (Calver, Hall et al. 1998). Immunofluorescent
174 and qRT-PCR results indicated increase of NG2 glia density in PDGFAA-treated COCS com-
175 pared to controls (**Fig. 3d-f**). We found that increase of NG2 glia number decreased the ex-
176 pression levels of both Cox2 and Ptges (**Fig. 3f**). These data indicate that NG2 glia regulate

177 the PGE2 biosynthesis pathway. In line with the above findings, upregulation of both Cox2
178 and Ptges were also observed in NG2-glia-depleted COCS after prion infection (**Fig. 3g**). As
179 comparison, we found that neither Cox1 nor Ptgds changed upon NG2 glia depletion (**Sup-**
180 **plementary Fig. 9**).
181 To investigate whether loss of NG2 glia induces similar changes of Cox2 and Ptges in vivo,
182 we examined the expression levels of Cox2 and Ptges as well as their cellular localization in
183 the brain by immunofluorescence. We found that the immunoreactivity of both Cox2 and Ptges
184 were relatively low under normal condition (**Fig. 3h-i**); however, prion infection increased their
185 expression levels (**Fig. 3h-i**), especially in microglia (**Fig. 3h**). Furthermore, NG2 glia depletion
186 increased prion-induced upregulation of Cox2 and Ptges (**Fig. 3j-k**), suggesting that NG2 glia
187 also regulate this pathway in vivo.
188
189 *NG2 glia regulate microglial PGE2 pathway through multiple mechanisms*
190 To molecularly characterize PGE2-producing microglia in prion-infected brains, we analyzed
191 a previously generated single-cell RNA sequencing dataset (Slota, Sajesh et al. 2022) based
192 on a prion infection model similar to that used in the current study. In normal brains, microglia
193 were largely (~99%) Cox2$^-$ or Ptges$^-$; however, the fractions of Cox2$^+$ and Ptges$^+$ microglia
194 were increased after prion infection in both the cerebral cortex (**Fig. 4a-b**) and hippocampus
195 (**Supplementary Fig. 10a-b**). Expression analysis identified 943 differentially expressed
196 genes (DEGs) between Cox2$^+$ and Cox2$^-$ microglia (**Supplementary table 1**), and 847 DEGs
197 between Ptges$^+$ and Ptges$^-$ microglia **(Supplementary table 2**), respectively, in the cerebral
198 cortex of prion-infected mice (**Fig. 4c**). The majority (~80%-90%) of DEGs identified in Cox2$^+$
199 microglia were also dysregulated in Ptges$^+$ microglia (**Fig. 4c**), suggesting that Cox2$^+$ and
200 Ptges$^+$ microglia largely overlap. Similar results were also observed in the hippocampus of
201 prion-infected mice (**Supplementary Fig. 10c, Supplementary table 3** and **Supplementary**
202 **table 4**).
203 The signature genes of homeostatic microglia, including Tmem119, P2ry12 and Cx3cr1, were
204 downregulated in Cox2$^+$/Ptges$^+$ microglia (**Fig. 4d** and **Supplementary Fig. 10d**), whereas
205 disease-associated microglia (DAM) (Keren-Shaul, Spinrad et al. 2017) signature genes such
206 as Itgax, Cst7 and Apoe as well as MHC$^+$ microglia (Mathys, Adaikkan et al. 2017) signature
207 genes such as H2-D1, H2-Aa and Cd74 were upregulated in Cox2$^+$/Ptges$^+$ microglia (**Fig. 4d**
208 and **Supplementary Fig. 10d**). No interferon response microglia (Mathys, Adaikkan et al.
209 2017) signature genes were significantly altered in Cox2$^+$/Ptges$^+$ microglia (**Fig. 4d**). In addi-
210 tion, we found that Cox2$^+$/Ptges$^+$ microglia expressed higher levels of inflammatory genes
211 (**Fig. 4d** and **Supplementary Fig. 10d**). These data suggest that Cox2$^+$/Ptges$^+$ microglia rep-
212 resent either a novel microglia population or a mixture of different microglia populations that
213 are involved in neurodegenerative diseases.

214 To investigate the mechanisms by which NG2 glia influence the generation of Cox2$^+$/Ptges$^+$
215 microglia in prion disease, we analyzed the cell-cell communication between NG2 glia and
216 Cox2$^+$ or Cox2$^-$ microglia at the single-cell level with CellChat (Jin, Guerrero-Juarez et al.
217 2021). We found that the number of interactions between NG2 glia and Cox2$^+$ or Cox2$^-$ micro-
218 glia was unchanged (**Fig. 4e** and **Supplementary Fig. 10d**). However, the strength of inter-
219 actions between NG2 glia and Cox2$^+$ microglia was weakened compared to NG2 glia and
220 Cox2$^-$ microglia (**Fig. 4e**). The weakened NG2 glia inputs on Cox2$^+$ microglia were associated
221 with multiple mechanistic categories, including secreted signaling such as transforming growth
222 factor beta 2 (Tgfb2), pleiotrophin (Ptn) and midkine (Mdk), ECM-receptor interaction such as
223 tenascin R (Tnr), laminin subunit gamma 1 (Lamc1) and collagen type IX alpha 3 chain
224 (Col9a3), and cell-cell contact such as vascular cell adhesion protein 1 (Vcam1), nectin cell
225 adhesion molecule 3 (Nectin3) and junctional adhesion molecule 3 (Jam3) (**Fig. 4f** and **Sup-**
226 **plementary Fig. 10f**).
227 We previously reported that Tgfb signaling disruption in NG2-glia-depleted COCS may be re-
228 sponsible for the loss of homeostatic microglia state (Liu and Aguzzi 2020). These observa-
229 tions not only validate the Cellchat analysis results (**Fig. 4f** and **Supplementary Fig. 10f**), but
230 also suggest that some of the weakened NG2 glia to Cox2$^+$ microglia signaling might be caus-
231 ally linked to the enhanced cellular state transition from Cox2$^-$ microglia into Cox2$^+$ microglia
232 in the NG2-glia-depleted mouse brains after prion infection. To test this hypothesis, we estab-
233 lished high-purity serum-free microglia cultures from mouse brains through Cd11b im-
234 munopanning (**Supplementary Fig. 11a-b**). After three days in culture, we treated primary
235 microglia with several of the NG2-glia-derived factors identified by the cell-cell communication
236 analysis (**Fig. 4f** and **Supplementary Fig. 10f**), including Tgfb2, Ptn, Mdk, bone morphoge-
237 netic protein 7 (Bmp7) and semaphorin3d (Sema3d) in the presence or absence of prions,
238 and examined Ptges levels with immunofluorescence. We found that Tgfb2, Ptn, Mdk but not
239 Bmp7 and Sema3d suppressed microglial Ptges expression under both experimental condi-
240 tions (**Fig. 4g-i**). These data suggest that NG2 glia can directly influence microglial Cox2-
241 Ptges pathway through multiple mechanisms.
242
243 *Inhibition of PGE2 biosynthesis diminishes prion neurotoxicity and decelerates prion disease*
244 Although previous studies indicated that the level of PGE2 in the CSF was increased in prion
245 disease patients (Minghetti, Greco et al. 2000, Minghetti, Cardone et al. 2002), it is unclear
246 whether PGE2 plays a causal role in prion-induced neurodegeneration. To investigate this,
247 we treated normal and prion-infected COCS with PGE2, PGD2, or DMSO as control, and
248 examined neurodegeneration by NeuN immunofluorescence. PGE2 treatment had no effect
249 on neuronal survival under normal conditions but enhanced neuronal death in prion-infected
250 COCS (**Fig. 5a-b**). In contrast, prion-induced neurodegeneration in PGD2-treated COCS was

251 largely unaltered compared to DMSO (**Fig. 5a-b**). To investigate whether inhibition of PGE2
252 biosynthesis protects against prion-induced neurodegeneration, we treated normal and prion-
253 infected COCS with C118 or C934 (Larsson, Steinmetz et al. 2019), two high-selective Ptges
254 inhibitors. Both Ptges inhibitors reduced neurodegeneration in prion-exposed COCS (**Fig. 5c-**
255 **d**). These results suggest that PGE2 is a potent enhancer of prion neurotoxicity, and inhibition
256 of PGE2 biosynthesis is neuroprotective.
257 To investigate the effects of PGE2 biosynthesis inhibition on prion disease in vivo, we inocu-
258 lated Cox2Luc mice, in which the Cox2 gene was replaced with the coding sequence of lucif-
259 erase, and control mice with prions. We found that Cox2Luc mice survived longer than their
260 littermate controls after prion infection (**Fig. 5e**), suggesting that elevation of Cox2 and PGE2
261 production during prion disease are detrimental in vivo. In consistent with this, immunofluo-
262 rescent staining of Map2 demonstrated ameliorated prion-induced dendritic pathology in the
263 hippocampus of the Cox2Luc mice compared to controls (**Fig. 5f-g).**
264
265 *Inhibition of PGE2 biosynthesis rescues the enhanced neurodegeneration and accelerated*
266 *prion disease after NG2 glia depletion*
267 Next, we investigated whether the upregulation of Cox2 and Ptges and the subsequent in-
268 crease of PGE2 biosynthesis were responsible for the enhanced prion neurotoxicity and ac-
269 celerated prion disease after NG2 glia depletion. We examined neuronal survival upon inhibi-
270 tion of Ptges activity by C118 and C934 in normal and prion-infected COCS with or without
271 NG2 glia depletion. Consistent with the aforementioned findings (**Fig. 2a-b**), loss of NG2 glia
272 enhanced prion-induced neurodegeneration (**Fig. 6a-b**). However, this enhancement was
273 largely blocked by C118 and C934 treatment (**Fig. 6a-b**). These data suggest that the en-
274 hanced neurodegeneration in NG2-glia-depleted COCS is mediated by PGE2.
275 We then crossed Pdgfrα-CreER mice and iDTR mice with Cox2Luc mice to generate Pdg-
276 frα^{iDTR}/Cox2Luc mice. Pdgfrα-CreER/Cox2Luc and iDTR/Cox2Luc mice served as controls
277 (Ctrl/Cox2Luc). We infected Pdgfrα^{iDTR}/Cox2Luc and Ctrl/Cox2Luc mice with prions and com-
278 pared them to prion inoculated Pdgfrα^{iDTR} and genetically matched control mice (designated
279 as Pdgfrα^{iDTR}/WT and Ctrl/WT mice, respectively). All mice were treated with tamoxifen one
280 month before prion inoculation and injected with DT at 16 wpi. As expected, loss of NG2 glia
281 accelerated prion disease in Pdgfrα^{iDTR}/WT mice compared to Ctrl/WT mice (**Fig. 6c**). How-
282 ever, the accelerated prion disease in NG2-glia-depleted mice was almost completely rescued
283 in Pdgfrα^{iDTR}/Cox2Luc mice compared to Ctrl/Cox2Luc mice (**Fig. 6c**), and both Pdg-
284 frα^{iDTR}/Cox2Luc mice and Ctrl/Cox2Luc mice survived longer than Pdgfrα^{iDTR}/WT and Ctrl/WT
285 mice (**Fig. 6c**). Loss of Cox2 also rescued the enhanced prion-induced dendritic pathology in
286 Pdgfrα^{iDTR}/Cox2Luc mice compared to Pdgfrα^{iDTR}/WT mice (**Fig. 6d-e**). These findings confirm

287 that increased PGE2 biosynthesis underlies the enhanced prion neurotoxicity and accelerated
288 prion disease in NG2 glia deficient mice.
289
290 *PGE2 enhances prion neurotoxicity through the EP4 receptor*
291 To investigate how PGE2 promotes prion-induced neurodegeneration, we first examined the
292 cellular localization of its receptors, including prostaglandin E receptor 1 (Ptger1, also known
293 as EP1), Ptger2 (also known as EP2), Ptger3 (also known as EP3) and Ptger4 (also known
294 as EP4), in the adult mouse brain by immunofluorescence. We found that all four PGE2 re-
295 ceptors were expressed by neurons (**Supplementary Fig. 12**). To determine which receptor
296 might be responsible for the enhanced prion neurotoxicity, we expressed them one by one
297 together with GFP in HovS cells chronically infected with prions (Avar, Heinzer et al. 2020)
298 through lentiviral transduction, and examined death of HovS cells in the presence or absence
299 of PGE2. We found that the number of GFP^+ HovS cells were comparable between PGE2-
300 and DMSO-treated groups when Ptger2, Ptger3 or a control construct was expressed (**Fig.**
301 **7a-b**). However, expression of Ptger1 and Ptger4 reduced the survival of HovS cells in PGE2-
302 treated groups compared to DMSO-treated controls (**Fig. 7a-b**). Furthermore, we observed an
303 abnormal morphology of surviving HovS cells, characterized by retraction of cellular processes
304 and shrinkage of cell bodies, after PGE2 treatment only when Ptger1 and Ptger4 were ex-
305 pressed (**Fig. 7a**). Therefore, PGE2 may enhance prion-induced neurodegeneration through
306 activating Ptger1- and Ptger4-mediated signaling.
307 To further confirm the possible involvement of Ptger1 and Ptger4 in PGE2-mediated enhance-
308 ment of neurodegeneration after prion infection, we established primary neuronal cultures us-
309 ing cerebellum from C57BL/6J mice. Immunofluorescence indicated expression of both Ptger1
310 and Ptger4 in primary neurons (**Supplementary Fig. 13**). We infected primary neurons with
311 prion-containing brain homogenates at day 5, and treated them with different concentrations
312 of Ptger1 agonist 17-phenyl-trinor-PGE2 (17-pt-PGE2), Ptger4 agonist L902688 or control sol-
313 vents 10 days later for 48 hours. We found that L902688 enhanced the death of prion-infected
314 neurons and damages to neuronal processes in a concentration dependent manner (**Fig. 7c-**
315 **d**). High concentration of L902688 also induced neuronal death in the absence of prions (**Sup-**
316 **plementary Fig. 14a-b**), suggesting activation of Ptger4 signaling is highly toxic to neurons.
317 In contrast, we found that activation of Ptger1 with several concentrations of 17-pt-PGE2 had
318 no effects on neuronal survival in the presence of prions (**Supplementary Fig. 14c-d**). Simi-
319 larly, we found that activation of Ptger4 but not Ptger1 enhanced prion-induced neurodegen-
320 eration in COCS in a concentration-dependent manner (**Fig. 7e-f** and **Supplementary Fig.**
321 **15a-b**). These results confirm that PGE2 enhances prion-induced neurodegeneration primarily
322 by activating the Ptger4-mediated signaling.

Discussion

Oligodendrocyte lineage cells have long been considered as supportive components of the CNS and bystanders in neurogenerative diseases (Ettle, Schlachetzki et al. 2016). However, accumulating evidence suggest that this cell lineage may have additional functions other than producing myelin sheath (Funfschilling, Supplie et al. 2012, Liu and Zhou 2013, Fruhbeis, Kuo-Elsner et al. 2020), and may be actively involved in neurodegenerative processes (Lee, Morrison et al. 2012, Pandey, Shen et al. 2022). Here we found that loss of oligodendrocyte precursor cells unleashed a microglial pathway that is responsible for PGE2 biosynthesis, which enhances prion-induced neurotoxicity and accelerates prion disease in animal models (**Supplementary Fig. 16**). These data uncover a crucial role of oligodendrocyte precursor cells in a non-cell-autonomous interaction network during prion infection, and support a protective function of these cells during chronic neurodegeneration. Developing approaches that promote the beneficial activities of oligodendrocyte precursor cells may hold potential for novel disease-modifying therapies.

The study of functions of oligodendrocyte-lineage cells was limited by the lack of efficient and specific ways to manipulate them ex vivo and in vivo. To overcome this difficulty, we previously established experimental approaches to deplete oligodendrocyte precursor cells in cultured brain slices and in adult mouse brains (Liu and Aguzzi 2020), which formed the basis for the discoveries described here. Adaption of these tools to other models of neurodegeneration, such as AD and PD, would facilitate the investigations of disease-specific roles of oligodendrocyte precursor cells.

We found that depletion of oligodendrocyte precursor cells augmented the PGE2 biosynthesis pathway in cultured brain slices and adult mouse brains after prion infection, revealing a previously unknown regulatory mechanism of PGE2 signaling in the CNS. The role of PGE2 signaling in prion disease and prion-induced neurodegeneration was undefined, but PGE2 levels were found to be increased in the CSF of prion disease patients (Minghetti, Greco et al. 2000, Minghetti, Cardone et al. 2002). Our findings indicate that PGE2 signaling is a strong enhancer of prion neurotoxicity and a potent driver of prion disease development, which underlies the enhanced neurodegeneration and accelerated prion disease in mice deficient of oligodendrocyte precursor cells. Furthermore, we found that PGE2 enhanced prion-induced neurodegeneration through directly binding to its receptor EP4 on neuronal cells. These data suggest that Ptges inhibitors blocking PGE2 biosynthesis, such as C118 and C934 (Larsson, Steinmetz et al. 2019), which were tested in the current study, as well as EP4 signaling antagonists, may represent good drug candidates for the treatment of prion disease.

Microglia play important roles in prion disease pathogenesis (Zhu, Herrmann et al. 2016, Carroll, Race et al. 2018, Bradford, McGuire et al. 2022). Besides neurons, glial cells, especially activated microglia, also express PGE2 receptors (Bonfill-Teixidor, Otxoa-de-Amezaga

360 et al. 2017). Manipulation of PGE2 signaling in microglia influences their reaction in models of
361 neurodegeneration (Johansson, Pradhan et al. 2013, Woodling, Wang et al. 2014). Therefore,
362 in addition to directly acting on neurons, PGE2 may modulate microglial phenotypes through
363 autocrine signaling, and contribute to neurodegeneration indirectly.
364 We previously reported that oligodendrocyte precursor cells were required for maintaining the
365 homeostatic state of microglia in the adult mouse brain; however, their loss did not result in
366 microglia activation and neuroinflammation under normal conditions (Liu and Aguzzi 2020), in
367 contrast to NG2 glia depletion in rats (Nakano, Tamura et al. 2017). While we now confirm this
368 even in the context of prion infections, we found that deficiency of oligodendrocyte precursor
369 cells dysregulates the PGE2 biosynthesis pathway in microglia. Single-cell RNA sequencing
370 data indicate that PGE2-producing microglia exhibit the molecular features of previously re-
371 ported DAM (Keren-Shaul, Spinrad et al. 2017) and of MHC^+ microglia (Mathys, Adaikkan et
372 al. 2017) but not interferon responsive microglia (Mathys, Adaikkan et al. 2017), and express
373 higher levels of inflammatory genes. PGE2-producing microglia may represent a novel micro-
374 glia population of diseased brains, or a mixture of several different microglia populations iden-
375 tified previously. Profiling larger numbers of microglial cells in the prion-inoculated brain with
376 single-cell RNA sequencing in future studies may help clarify this crucial question.
377 Using CellChat (Jin, Guerrero-Juarez et al. 2021) to analyze NG2 glia-microglia communica-
378 tions in the prion-infected brain at the single-cell level, we identified multiple weakened NG2-
379 glia-to-microglia signals that might be mechanistically linked to the enhanced generation of
380 PGE2-producing microglia in NG2-glia-depleted brains after prion infection. Of these, we val-
381 idated Tgfb2, Ptn and Mdk experimentally in primary microglia cultures. Targeting these sig-
382 nals or other CellChat-identified NG2-glia-derived factors may represent promising ways for
383 modulating microglia phenotypes in neurodegenerative diseases.
384

385 **Materials and methods**

386 *Mouse experiments*

387 C57BL/6J mice were obtained from Charles River, Germany. Tga20 mice (Fischer, Rulicke et
388 al. 1996) were obtained from Laboratory Animal Services Center at University of Zurich, Swit-
389 zerland. Pdgfrα-CreER mice (Stock No: 018280), iDTR mice (Stock No: 007900) and Cox2Luc
390 mice (Stock No: 030853) were obtained from the Jackson Laboratory, USA. Double trans-
391 genic Pdgfrα-CreER/iDTR (Pdgfrα^{iDTR}) mice were generated by crossing the Pdgfrα-CreER
392 mice with the iDTR mice. To induce Cre activity and DTR expression in NG2 glia, Pdgfrα^{iDTR}
393 mice were fed with tamoxifen-containing diet (ENVIGO, TD. 55125.I) for 4 weeks as previously
394 reported (Liu and Aguzzi 2020). To generate Pdgfrα^{iDTR} mice on a Cox2Luc background, Pdg-
395 frα-CreER mice and iDTR mice were first crossed with the Cox2Luc mice, then the resulting
396 Pdgfrα-CreER mice and iDTR mice on the Cox2Luc background were crossed with each other.
397 Littermates of the experimental groups were used as controls. All animal experiments in the
398 current study were performed according to Swiss federal guidelines and had been approved
399 by the Animal Experimentation Committee of the Canton of Zurich under the permits 040/2015,
400 139/2016, 243/2018 and 236/2019.

401

402 *Prion inoculation*

403 Intracerebral prion inoculation was performed as previously described (Liu, Senatore et al.
404 2022). Briefly, adult mice were anesthetized with isoflurane and injected in the right hemi-
405 sphere of the brain with 30 μl 0.01% w/v brain homogenates derived from adult C57BL/6J
406 mice suffering from terminal prion disease. Prion strain used in the current study was the
407 Rocky Mountain Laboratory strain of scrapie, passage 6. Mice inoculated with 30 μl 0.01%
408 w/v non-infectious brain homogenates were used as controls. After prion inoculation, the
409 health status of mice was closely monitored, and body weights of mice were recorded once
410 per week. For experiments evaluating survival time, mice were euthanized when showing ter-
411 minal disease symptoms or reached more than 20% loss of body weight. For biochemical and
412 immunohistochemical analysis, mice were euthanized at specific time points after prion inoc-
413 ulation for tissue collection. To avoid potential influences of tamoxifen on prion disease devel-
414 opment, mouse strains (e.g., Pdgfrα-CreER, iDTR and Pdgfrα^{iDTR} mice on WT or Cox2Luc
415 background) went through tamoxifen food treatment was inoculated at least 4 weeks after
416 switching back to the normal diet.

417

418 *Cerebellar organotypic cultured slices (COCS)*

419 COCS were prepared according to a previously published protocol (Falsig and Aguzzi 2008).
420 Briefly, cerebella from 12-day old C57BL/6J or Tga20 pups were dissected, embedded in low

421 melting point agarose (Invitrogen, 15517-022) and cut into 350-μm thick slices with a vi-
422 bratome (Leica, VT1000S) in cold Gey's balanced salt solution (GBSS) supplemented with the
423 glutamate receptor antagonist kynurenic acid (1 mM, Sigma, K3375) and glucose (33.33 mM,
424 Sigma, G8769). Slices with intact morphology were collected and briefly washed 3 times in
425 GBSS supplemented with kynurenic acid and glucose. Afterwards, brain slices were exposed
426 to either 0.01% w/v prion-containing brain homogenates or 0.01% w/v brain homogenates
427 derived from healthy mice for 1 hour at 4 °C and washed 5 times in GBSS supplemented with
428 kynurenic acid and glucose. Six to eight slices were put on a Millicell-CM Biopore PTFE mem-
429 brane insert (Millipore, PICM 03050) and kept on slice culture medium containing 50% MEM,
430 25% BME, 25% inactivated horse serum, 0.65% w/v glucose, 1% GlutaMax (ThermoFisher
431 Scientific, 35050061) and 1% penicillin/streptomycin (ThermoFisher Scientific, 10378016) at
432 37 °C in a tissue culture incubator. Culture medium was changed 3 times per week.
433
434 *Treatment of brain slice cultures*
435 Prostaglandin E2 (PGE2, sc-201225), prostaglandin D2 (PGD2, sc-201221) and EP1 receptor
436 agonist 17-Phenyl-trinor-prostaglandin E2 (17-pt-PGE2, sc-201255) were purchased from
437 Santa Cruz Biotechnology. EP4 receptor agonist L902688 (HY-119163) was purchased from
438 MedChemExpress. Prostaglandin E synthase (Ptges) inhibitors C118 and C934 (Larsson,
439 Steinmetz et al. 2019) were obtained from Dr. Per-Johan Jakobsson at Karolinska Institutet,
440 Sweden. All the above compounds except L902688, which was dissolved in methanol, were
441 dissolved in DMSO (Sigma, 472301) and stored at −80 °C in aliquots. Treatments of COCS
442 with PGE2 (1 μM), PGD2 (1 μM), C118 (2 μM) and C934 (2 μM), 17-pt-PGE2 (1 μM and 5
443 μM) and L902688 (1 μM and 5 μM) were started from 14 days after the cultures were estab-
444 lished and lasted to the end of experiments. COCS treated with same amounts of DMSO (or
445 methanol for L902688) were used as controls. Recombinant human PDGFAA (110-13A) was
446 purchased from Peprotech, dissolved in Opti-MEM, and stored at -20 °C in aliquots. Treatment
447 of COCS with PDGFAA (40 ng/ml) was performed following the same protocol as with the
448 compounds, except that COCS treated with Opti-MEM were used as controls.
449
450 *NG2 glia depletion*
451 NG2 glia depletion in COCS and in vivo was performed as previously described (Liu and
452 Aguzzi 2020). Briefly, to achieve ex vivo NG2 glia depletion, CP673451 (MedChemExpress,
453 HY-12050) was supplemented in slice culture medium with the concentration of 1 μM. Treat-
454 ments were started from 14 days after the cultures were established and lasted to the end of
455 experiments (for long-term continuous depletion) or 10 days (for short-term transient deple-
456 tion). Fresh CP673451 was added every time when the culture medium was changed. COCS

457 treated with same amounts of DMSO were used as controls. To achieve in vivo NG2 glia
458 depletion, tamoxifen-treated Pdgfrα^{iDTR} mice were injected intraperitoneally with diphtheria
459 toxin (DT, Sigma, D0564) diluted in saline for five consecutive days (two injections per day
460 with an 8-hour interval, 200 ng per injection). DT-injected tamoxifen-treated Pdgfrα-CreER
461 mice and iDTR mice were pooled together and used as controls.
462
463 *Lentiviral production*
464 Lenti-vectors used for expressing human PGE2 receptors EP1 (pLenti-PTGER1-mGFP-P2A-
465 Puro, RC208597L4), EP2 (pLenti-PTGER2-mGFP-P2A-Puro, RC210883L4), EP3 (pLenti-
466 PTGER3-mGFP-P2A-Puro, RC220173L4) and EP4 (pLenti-PTGER4-mGFP-P2A-Puro,
467 RC210932L4) were purchased from OriGene Technologies. A control vector (pLenti-HygR-
468 mGFP-P2A-Puro) was produced in house by replacing the EP2 sequence in the pLenti-
469 PTGER2-mGFP-P2A-Puro plasmid with the sequence of the Hygromycin resistant gene
470 (HygR). All plasmids were verified by Sanger sequencing before lentiviral production in
471 HEK293T cells maintained in Opti-MEM supplemented with 10% fetal bovine serum (FBS).
472 Briefly, HEK293T cells were seeded in 10-cm cell culture dishes and transfected at ~ 80%
473 confluency with a packaging plasmid mixture (transgene plasmid; VSVG plasmid; PAX2 plas-
474 mid) using FuGENE HD transfection reagent (Promega, E2311). Twenty-four hours after
475 transfection, culture medium was changed to remove the transfection reagent. After another
476 48 hours, the culture medium containing lentivirus was collected, centrifuged at 1500g for 10
477 minutes and filtered through 0.45-micron Whatman filter units (GE Healthcare, 10462100).
478 High-titer lentivirus was produced by concentrating the filtered supernatant with Lenti-X con-
479 centrator (Takara, 631231) and stored at -80 °C in aliquots.
480
481 *Primary microglia culture*
482 Serum-free mouse microglia cultures were established using the immunopanning method ac-
483 cording to previously published protocols with small modifications. Briefly, brain tissues (olfac-
484 tory bulb, cerebellum and subcortical regions removed) from 5-day old C57BL/6J mice were
485 dissected in cold Hanks' Balanced Salt solution (HBSS, TermoFisher Scientific, 14175095)
486 under a stereomicroscope. After removing meninges, brain tissues were minced and washed
487 three times with HBSS. Afterwards, the minced brain tissues were digested in papain solution
488 (Worthington Biochemical Corporation, LK003178) with DNase1 (Worthington Biochemical
489 Corporation, LK003172) for 20 minutes at 37 °C and pipetted into single-cell suspension. The
490 digestion solution was removed through centrifugation (1000g for 5 minutes), and cell pellets
491 were resuspended in OptiMEM and filtered through a 70-μm cell strainer for immnopanning at
492 room temperature. Each Petri dish used for immnopanning was coated with 30 μl goat anti-
493 rat IgG (Jackson ImmunoResearch 112-005-167) diluted in 10 ml of sterile 50 mM Tris-HCl

494 (pH 9.5) overnight at 4 °C. After 5 times of washing in phosphate buffered saline (PBS), the
495 dishes were further coated with 30 µl rat anti-mouse CD11b antibody (ThermoFisher Scientific,
496 14-0112-82) diluted in the same buffer overnight at 4 °C and washed 5 times in PBS before
497 use. After immunopanning for 45 minutes (gently swirl the dishes every 15 minutes), the float-
498 ing cells in the suspension were removed from the dishes, and cells attached to the dishes
499 were washed 5 times with PBS and digested with trypsin-EDTA (ThermoFisher Scientific,
500 25200056) for 10 minutes at 37 °C. Afterwards, the cells were collected by centrifugation,
501 resuspended, and seeded in ibiTreat 8-well slide chambers (Ibidi, 80806) in OptiMEM-based
502 medium containing 1% Sato Mix, 1% GlutaMax, 1% penicillin/streptomycin, 2 ng/ml human
503 Tgfb2 (ThermoFisher Scientific, 100-35B), 10 ng/ml murine Csf1 (Biolegend, 576404) and 1.5
504 mg/ml cholesterol (Merck, C3045). After 3 days in culture, primary microglia were treated with
505 recombinant human Tgfb2 (100 ng/ml), human Pleiotrophin (100 ng/ml, ThermoFisher Scien-
506 tific, 450-15), human Midkine (100 ng/ml, ThermoFisher Scientific, 450-16), human Bmp7 (100
507 ng/ml, ThermoFisher Scientific, 120-03P) or human Semaphorin3d (400 ng/ml, Novus Biolog-
508 icals, H00223117-P01) for 72 hours in the presence or absence of 0.01% w/v prion-containing
509 brain homogenates, followed by PFA fixation and immunofluorescence.
510
511 *Primary neuronal culture*
512 Primary neuronal cultures were established using cerebellar tissues from 5-day old C57BL/6J
513 mice according to previously published protocols. Briefly, after removing meninges, cerebellar
514 tissues were minced, washed three times with HBSS, digested in papain solution with DNase1
515 for 15 minutes at 37 °C and pipetted into single-cell suspension. After centrifugation, cell pel-
516 lets were resuspended in OptiMEM and incubated in uncoated tissue culture dishes for 10 min
517 to remove astrocytes and microglia. Afterwards, the cells were recollected, centrifuged, resus-
518 pended in neuronal culture medium containing Neurobasal medium (ThermoFisher Scientific,
519 21103049), 1% N2 (ThermoFisher Scientific, 17502048), 1% B27 (ThermoFisher Scientific,
520 17504044), 1% MEM Non-Essential Amino Acids (MEM NEAA, ThermoFisher Scientific,
521 11140050), 1% GlutaMax and 1% penicillin/streptomycin, and seeded in 48-well plates coated
522 with PDL (ThermoFisher Scientific, A3890401). After 1 day, the cultures were treated with 2
523 µM AraC (British Pharmacopoeia, 383) for 24 hours to further remove glial cells. For prion
524 infection, 0.01% w/v prion-containing brain homogenates were added into the cultures at day
525 5. After 10 days of prion infection, the cultures were treated with different concentrations of
526 17-pt-PGE2 and L902688 for 48 hours or controls (DMSO for 17-pt-PGE2 and methanol for
527 L902688), followed by fixation and immunofluorescence.
528
529 *HovS cell culture*

530 HovS cells (Avar, Heinzer et al. 2020), a subclone of the human SH-SY5Y cell line, where the
531 human PRNP gene was replaced with the ovine PRNP VRQ allele, were maintained in
532 OptMEM medium supplemented with 10% FBS, 1% MEM-NEAA, 1% GlutaMax, 1% penicil-
533 lin/streptomycin and 400 μg/ml Geneticin (ThermoFisher Scientifc, 10131027). To establish a
534 cellular model of chronic prion infection, HovS cells were exposed to brain homogenates de-
535 rived from PG127-prion-infected tg338 mice and passaged for at least 10 times before being
536 used for experiments. To investigate the effects of PGE2 and the involved PGE2 receptors in
537 prion-induced cell toxicity, PG127-HovS cells were seeded into 96-well plates. Twenty-four
538 hours after seeding, cells were transduced with either control lentivirus or lentivirus harboring
539 one of the four EP receptor transgenes. After 48 hours, the lentivirus-containing culture me-
540 dium was removed, and fresh culture medium supplemented with DMSO or PGE2 (10 μM)
541 was added in the wells and incubated for another 48 hours. Finally, GFP^+ cells (cells infected
542 by lentivirus) were imaged with a Nikon Eclipse Ti2-E fluorescent microscope and quantified
543 with ImageJ.
544
545 *Western blotting*
546 Western blotting was performed as previously described (Liu, Sorce et al. 2018). Briefly, cul-
547 tured brain slices or collected brain tissues were lysed with a bead-mill homogenizer in RIPA
548 buffer supplemented with proteinase inhibitor cocktail cOmplete (MERCK, 11697498001) and
549 phosphatase inhibitor cocktail PhosSTOP (MERCK, 4906845001). After centrifuge, protein
550 concentrations in the supernatant were quantified with the BCA method. Protein samples were
551 then mixed with western blotting loading buffer and boiled for 5 minutes at 95 °C before being
552 loaded onto gels. For western blotting aimed to detect prions, samples were first digested with
553 10 μg/ml (for COCS) or 20 μg/ml (for brain tissues) proteinase K for 30 minutes at 37 °C, then
554 mixed with western blotting loading buffer and boiled for 5 minutes at 95 °C. The following
555 primary antibodies were used: mouse monoclonal antibody against actin (1:10,000, Merck
556 Millipore, MAB1501R); mouse monoclonal antibody against PrP (POM1, 1:5000, homemade);
557 rabbit polyclonal antibody against NG2 (1:500, MERCK, AB5320); rabbit polyclonal antibody
558 against PDGFRα (1:500, Santa Cruz, sc-338); rabbit monoclonal antibody against NeuN
559 (1:2000, Abcam, ab177487). Depending on the primary antibodies used, suitable HRP-conju-
560 gated secondary antibodies (1:10,000, Jackson ImmunoResearch Laboratories) were chosen.
561 Membranes were developed with Crescendo Western HRP Substrate (MERCK,
562 WBLUR0500), visualized, and digitized with ImageQuant (LAS-4000; Fujifilm, Japan). Optical
563 densities of bands were analyzed using ImageJ.
564
565 *Immunofluorescence*

566 Immunofluorescent staining of cultured brain slices, primary cells and cryosections was per-
567 formed according to procedures published previously (Liu and Aguzzi 2020). For cultured brain
568 slices: after removing culture medium, brain slices were washed with PBS and fixed in 4%
569 PFA for 30 min at room temperature. After several washes to remove residual PFA, brain
570 slices were then permeabilized with PBST (PBS + 0.1% Triton X-100) for 2 hours at room
571 temperature and blocked with 5% goat serum (GS) overnight at 4 °C before adding primary
572 antibodies. For primary cells: after removing culture medium, cells were washed with PBS and
573 fixed in 4% PFA for 30 min at room temperature. After several washes to remove residual
574 PFA, cells were blocked with 5% GS for 2 hours at room temperature before adding primary
575 antibodies. For cryosections: mice were perfused transcardially with 20 ml PBS and 20 ml 4%
576 PFA. The dissected brains were then postfixed with 4% PFA for 4 hr or overnight in the fridge.
577 After removing PFA and brief washing with PBS, brains were transferred into 30% sucrose
578 solution for dehydration, and kept at 4°C. After dehydration was complete, brains were cut into
579 25-μm thick cryosections. To perform immunostaining, cryosections were permeabilized in
580 PBST for 2 hours and blocked with 5% GS for 2 hours at room temperature before incubation
581 in primary antibodies. The following primary antibodies were used: rabbit polyclonal antibody
582 against NG2 (1:500, a gift from Prof. Stallcup), rabbit monoclonal antibody against NeuN
583 (1:1000, Abcam, ab177487), rabbit polyclonal antibody against Iba1 (1:500, Wako, 019-
584 19741), rat monoclonal antibody against Cd68 (1:200, BioRad, MCA1957), rabbit polyclonal
585 antibody against Map2 (1:200, Biolegend, 840601), mouse monoclonal antibody against Tau
586 (1:200, ThermoFisher Scientific, MN1010), chicken polyclonal antibody against NeuN (1:1000,
587 Merck, ABN91), mouse monoclonal antibody against Cox2 (1:200, Santa Cruz, sc-166475),
588 mouse monoclonal antibody against Ptges (1:200, Santa Cruz, sc-365844), rabbit polyclonal
589 antibody against EP1 (1:200, Bioss Antibodies, BS-6316R), rabbit monoclonal antibody
590 against EP2 (1:200, Abcam, ab167171), rabbit polyclonal antibody against EP3 (1:200, Cay-
591 man Chemical, 101760) and mouse monoclonal antibody against EP4 (1:200, ProteinTech,
592 66921-1-Ig). Cultured brain slices were incubated in primary antibody at 4°C for 3 days. Cry-
593 osections and primary cells were incubated in primary antibody at 4°C overnight. After several
594 washes in PBST, cultured brain slices were incubated in suitable secondary antibodies over-
595 night at 4°C, and cryosections and primary cells were incubated in suitable secondary anti-
596 bodies for 2 hours at room temperature. Immunofluorescent images were captured using a
597 FLUOVIEW FV10i confocal microscope (Olympus Life Science) or Nikon Eclipse Ti2-E fluo-
598 rescent microscope, and were quantified using ImageJ.
599
600 *Quantitative real-time PCR*
601 To perform quantitative real-time-PCR (qRT-PCR) analysis, total RNA from cultured brain
602 slices or collected brain tissues was extracted using TRIzol reagent (ThermoFisher Scientific,

603 15596026). QuantiTect Reverse Transcription kit (QIAGEN, 205311) was used to synthesize
604 cDNA from the extracted RNA samples. qRT-PCR was performed on a ViiA7 Real-Time PCR
605 system (Applied Biosystems, USA) using the SYBR Green PCR Master Mix (ThermalFisher
606 Scientifc, 4309155). We used the following primers for qRT-PCR analysis: Mouse actin:
607 sense, 5′-AGATCAAGATCATTGCTCCTCCT-3′, antisense, 5′-ACGCAGCTCAGTAACAG-
608 TCC-3′. Mouse NG2: sense, 5′-ACCCAGGCTGAGGTAAATGC-3′, antisense, 5′-
609 ACAGGCAGCATCGAAAGACA-3′. Mouse Pdgfrα: sense, 5′-ATTAAGCCGGTCCCAACCTG-
610 3′, antisense, 5′-AATGGGACCTGACTTGGTGC-3′. Mouse TNFα: sense, 5′-ACGTCGTAG-
611 CAAACCACCAA-3′, antisense, 5′-ATAGCAAATCGGCTGACGGT-3′. Mouse IL1β: sense, 5′-
612 TGCAGCTGGAGAGTGTGGATCCC-3′, antisense, 5′-TGTGCTCTGCTTGTGAGGTGCTG-
613 3′. Mouse IL12β: sense, 5′-TGGTTTGCCATCGTTTTGCTG-3′, antisense, 5′-
614 ACAGGTGAGGTTCACTGTTTCT-3′. Mouse Cox1: sense, 5′-TCCATCCACTCCCAGAG-
615 TCAT-3′, antisense, 5′-ACAACAGGGATTGACTGGTGA-3′. Mouse Cox2: sense, 5′-
616 GGGCCATGGAGTGGACTTAAA-3′, antisense, 5′-ACTCTGTTGTGCTCCCGAAG-3′. Mouse
617 Ptges: sense, 5′-TCTCACTCTCAGTCCCGGTG-3′, antisense, 5′-GGGGTTGGCAAAA-
618 GCCTTC-3′. Mouse Ptgds: sense, 5′-GCTCCTTCTGCCCAGTTTTCC-3′, antisense, 5′-
619 CCCCAGGAACTTGTCTTGTTGA-3′.
620
621 *Single-cell RNA sequencing analysis*
622 Cerebral cortex and hippocampal single-cell RNA sequencing dataset from prion-infected or
623 control mice (Slota, Sajesh et al. 2022) were obtained from the single cell portal at the Broad
624 institute through the following link: https://singlecell.broadinstitute.org/sin-
625 gle_cell/study/SCP1962. After loading the raw single-cell RNA sequencing data into R, dou-
626 blets and ambient RNA were removed using scrublet (Wolock, Lopez et al. 2019) and decontX
627 (Yang, Corbett et al. 2020), respectively. Cells with nFeature_RNA less than 1000 or more
628 than 7000 or mitochondrial RNA percentage more than 5% were filtered out using Seurat
629 (Stuart, Butler et al. 2019). After normalizing the data and regressing out the mitochondrial
630 genes and cell cycle effects with Seurat, data from different animals were integrated using
631 Harmony (Korsunsky, Millard et al. 2019). After data integration, cells were clustered using
632 UMAP, and the resulting clusters were annotated based on known cell-type markers. To mo-
633 lecularly characterize $Cox2^+$ and $Ptges^+$ microglia populations in the prion-infected mouse
634 brain, microglia clusters were selected for further analysis, and differentially expressed genes
635 between the $Cox2^+$ and $Cox2^-$ or $Ptges^+$ and $Ptges^-$ microglia were identified using the Find-
636 Markers function in Seurat based on the cutoff FDR < 0.05 and logfc.threshold > 0.25.
637 Changes of cell-cell interactions between NG2 glia and $Cox2^+$ or $Cox2^-$ microglia at the single-
638 cell level in the prion-infected mouse brain were analyzed using the CellChat package (Jin,
639 Guerrero-Juarez et al. 2021).

Statistical analyses

Unless otherwise mentioned, unpaired, two-tailed student's t test was used for comparing data from two groups. All data were presented as mean ± SEM. To compare the incubation time of prion-inoculated mice, survival curves were estimated using the Kaplan-Meier method and compared statistically using the log rank test. Statistical analysis and data visualization were done using GraphPad Prism 9. P-value < 0.05 was considered statistically significant.

Acknowledgements

We thank Dr. William Stallcup for providing the polyclonal antibodies against NG2, Julie Domange, Mirzet Delic, Maria Svercelova and Marija Mihailova for excellent assistance. YL was supported by a Forschungskredit PostDoc grant (FK Liu 19-042). AA was supported by an Advanced Grant of the European Research Council (ERC 670958), the Swiss National Foundation (SNF 179040), and the Nomis Foundation.

Author Contributions

YL and AA conceptualized the study. YL designed and performed the experiments with help from JG, MM and MK. PJ provided the Ptges inhibitors and helpful guidance on relevant experiments. YL and AA wrote the manuscript.

Declaration of Interests

The authors declare no competing interest.

662 **Reference**

663 Aguzzi, A. and Y. Liu (2017). "A role for astroglia in prion diseases." J Exp Med **214**(12): 3477-
664 3479.
665 Akhtar, S., A. Wenborn, S. Brandner, J. Collinge and S. E. Lloyd (2011). "Sex effects in mouse
666 prion disease incubation time." PLoS One **6**(12): e28741.
667 Alonso, G. (2005). "NG2 proteoglycan-expressing cells of the adult rat brain: possible
668 involvement in the formation of glial scar astrocytes following stab wound." Glia **49**(3): 318-
669 338.
670 Avar, M., D. Heinzer, N. Steinke, B. Dogancay, R. Moos, S. Lugan, C. Cosenza, S. Hornemann,
671 O. Andreoletti and A. Aguzzi (2020). "Prion infection, transmission, and cytopathology
672 modeled in a low-biohazard human cell line." Life Sci Alliance **3**(8).
673 Bonfill-Teixidor, E., A. Otxoa-de-Amezaga, M. Font-Nieves, M. G. Sans-Fons and A. M. Planas
674 (2017). "Differential expression of E-type prostanoid receptors 2 and 4 in microglia stimulated
675 with lipopolysaccharide." J Neuroinflammation **14**(1): 3.
676 Bradford, B. M., L. I. McGuire, D. A. Hume, C. Pridans and N. A. Mabbott (2022). "Microglia
677 deficiency accelerates prion disease but does not enhance prion accumulation in the brain."
678 Glia **70**(11): 2169-2187.
679 Brandner, S., S. Isenmann, A. Raeber, M. Fischer, A. Sailer, Y. Kobayashi, S. Marino, C.
680 Weissmann and A. Aguzzi (1996). "Normal host prion protein necessary for scrapie-induced
681 neurotoxicity." Nature **379**(6563): 339-343.
682 Brandner, S. and Z. Jaunmuktane (2017). "Prion disease: experimental models and reality."
683 Acta Neuropathol **133**(2): 197-222.
684 Bueler, H., A. Aguzzi, A. Sailer, R. A. Greiner, P. Autenried, M. Aguet and C. Weissmann (1993).
685 "Mice devoid of PrP are resistant to scrapie." Cell **73**(7): 1339-1347.
686 Calver, A. R., A. C. Hall, W. P. Yu, F. S. Walsh, J. K. Heath, C. Betsholtz and W. D. Richardson
687 (1998). "Oligodendrocyte population dynamics and the role of PDGF in vivo." Neuron **20**(5):
688 869-882.
689 Carroll, J. A., B. Race, K. Williams, J. Striebel and B. Chesebro (2018). "Microglia Are Critical in
690 Host Defense against Prion Disease." J Virol **92**(15).
691 Chen, W. T., A. Lu, K. Craessaerts, B. Pavie, C. Sala Frigerio, N. Corthout, X. Qian, J. Lalakova,
692 M. Kuhnemund, I. Voytyuk, L. Wolfs, R. Mancuso, E. Salta, S. Balusu, A. Snellinx, S. Munck, A.
693 Jurek, J. Fernandez Navarro, T. C. Saido, I. Huitinga, J. Lundeberg, M. Fiers and B. De Strooper
694 (2020). "Spatial Transcriptomics and In Situ Sequencing to Study Alzheimer's Disease." Cell
695 **182**(4): 976-991 e919.
696 Dimitriadis, A., F. Zhang, T. Murphy, T. Trainer, Z. Jaunmuktane, C. Schmidt, T. Nazari, J.
697 Linehan, S. Brandner, J. Collinge, S. Mead and E. Viré (2022). "Single-nuclei transcriptomics of
698 mammalian prion diseases identifies dynamic gene signatures shared between species."
699 bioRxiv: 2022.2009.2013.507650.
700 Ettle, B., J. C. M. Schlachetzki and J. Winkler (2016). "Oligodendroglia and Myelin in
701 Neurodegenerative Diseases: More Than Just Bystanders?" Mol Neurobiol **53**(5): 3046-3062.
702 Falsig, J. and A. Aguzzi (2008). "The prion organotypic slice culture assay--POSCA." Nat Protoc
703 **3**(4): 555-562.
704 Fischer, M., T. Rulicke, A. Raeber, A. Sailer, M. Moser, B. Oesch, S. Brandner, A. Aguzzi and C.
705 Weissmann (1996). "Prion protein (PrP) with amino-proximal deletions restoring
706 susceptibility of PrP knockout mice to scrapie." EMBO J **15**(6): 1255-1264.

707 Fruhbeis, C., W. P. Kuo-Elsner, C. Muller, K. Barth, L. Peris, S. Tenzer, W. Mobius, H. B. Werner,
708 K. A. Nave, D. Frohlich and E. M. Kramer-Albers (2020). "Oligodendrocytes support axonal
709 transport and maintenance via exosome secretion." PLoS Biol **18**(12): e3000621.
710 Fuhrmann, M., G. Mitteregger, H. Kretzschmar and J. Herms (2007). "Dendritic pathology in
711 prion disease starts at the synaptic spine." J Neurosci **27**(23): 6224-6233.
712 Funfschilling, U., L. M. Supplie, D. Mahad, S. Boretius, A. S. Saab, J. Edgar, B. G. Brinkmann, C.
713 M. Kassmann, I. D. Tzvetanova, W. Mobius, F. Diaz, D. Meijer, U. Suter, B. Hamprecht, M. W.
714 Sereda, C. T. Moraes, J. Frahm, S. Goebbels and K. A. Nave (2012). "Glycolytic
715 oligodendrocytes maintain myelin and long-term axonal integrity." Nature **485**(7399): 517-
716 521.
717 Jin, S., C. F. Guerrero-Juarez, L. Zhang, I. Chang, R. Ramos, C. H. Kuan, P. Myung, M. V. Plikus
718 and Q. Nie (2021). "Inference and analysis of cell-cell communication using CellChat." Nat
719 Commun **12**(1): 1088.
720 Jin, X., T. R. Riew, H. L. Kim, J. H. Choi and M. Y. Lee (2018). "Morphological characterization
721 of NG2 glia and their association with neuroglial cells in the 3-nitropropionic acid-lesioned
722 striatum of rat." Sci Rep **8**(1): 5942.
723 Johansson, J. U., S. Pradhan, L. A. Lokteva, N. S. Woodling, N. Ko, H. D. Brown, Q. Wang, C.
724 Loh, E. Cekanaviciute, M. Buckwalter, A. B. Manning-Bog and K. I. Andreasson (2013).
725 "Suppression of inflammation with conditional deletion of the prostaglandin E2 EP2 receptor
726 in macrophages and brain microglia." J Neurosci **33**(40): 16016-16032.
727 Keren-Shaul, H., A. Spinrad, A. Weiner, O. Matcovitch-Natan, R. Dvir-Szternfeld, T. K. Ulland,
728 E. David, K. Baruch, D. Lara-Astaiso, B. Toth, S. Itzkovitz, M. Colonna, M. Schwartz and I. Amit
729 (2017). "A Unique Microglia Type Associated with Restricting Development of Alzheimer's
730 Disease." Cell **169**(7): 1276-1290 e1217.
731 Korsunsky, I., N. Millard, J. Fan, K. Slowikowski, F. Zhang, K. Wei, Y. Baglaenko, M. Brenner, P.
732 R. Loh and S. Raychaudhuri (2019). "Fast, sensitive and accurate integration of single-cell data
733 with Harmony." Nat Methods **16**(12): 1289-1296.
734 Larsson, K., J. Steinmetz, F. Bergqvist, S. Arefin, L. Spahiu, J. Wannberg, S. C. Pawelzik, R. Mor-
735 genstern, P. Stenberg, K. Kublickiene, M. Korotkova and P. J. Jakobsson (2019). "Biological
736 characterization of new inhibitors of microsomal PGE synthase-1 in preclinical models of
737 inflammation and vascular tone." Br J Pharmacol **176**(24): 4625-4638.
738 Lee, Y., B. M. Morrison, Y. Li, S. Lengacher, M. H. Farah, P. N. Hoffman, Y. Liu, A. Tsingalia, L.
739 Jin, P. W. Zhang, L. Pellerin, P. J. Magistretti and J. D. Rothstein (2012). "Oligodendroglia
740 metabolically support axons and contribute to neurodegeneration." Nature **487**(7408): 443-
741 448.
742 Liu, Y. and A. Aguzzi (2019). "Immunotherapy for neurodegeneration?" Science **364**(6436):
743 130-131.
744 Liu, Y. and A. Aguzzi (2020). "NG2 glia are required for maintaining microglia homeostatic
745 state." Glia **68**(2): 345-355.
746 Liu, Y., A. Senatore, S. Sorce, M. Nuvolone, J. Guo, Z. H. Gumus and A. Aguzzi (2022). "Brain
747 aging is faithfully modelled in organotypic brain slices and accelerated by prions." Commun
748 Biol **5**(1): 557.
749 Liu, Y., S. Sorce, M. Nuvolone, J. Domange and A. Aguzzi (2018). "Lymphocyte activation gene
750 3 (Lag3) expression is increased in prion infections but does not modify disease progression."
751 Sci Rep **8**(1): 14600.
752 Liu, Y. and J. Zhou (2013). "Oligodendrocytes in neurodegenerative diseases." Frontiers in
753 Biology **8**(2): 127-133.

754 Loeuillet, C., P. Y. Boelle, C. Lemaire-Vieille, M. Baldazza, P. Naquet, P. Chambon, M. F.
755 Cesbron-Delauw, A. J. Valleron, J. Gagnon and J. Y. Cesbron (2010). "Sex effect in mouse and
756 human prion disease." J Infect Dis **202**(4): 648-654.
757 Mathys, H., C. Adaikkan, F. Gao, J. Z. Young, E. Manet, M. Hemberg, P. L. De Jager, R. M.
758 Ransohoff, A. Regev and L. H. Tsai (2017). "Temporal Tracking of Microglia Activation in
759 Neurodegeneration at Single-Cell Resolution." Cell Rep **21**(2): 366-380.
760 Mathys, H., J. Davila-Velderrain, Z. Peng, F. Gao, S. Mohammadi, J. Z. Young, M. Menon, L. He,
761 F. Abdurrob, X. Jiang, A. J. Martorell, R. M. Ransohoff, B. P. Hafler, D. A. Bennett, M. Kellis and
762 L. H. Tsai (2019). "Single-cell transcriptomic analysis of Alzheimer's disease." Nature
763 **570**(7761): 332-337.
764 Minghetti, L., F. Cardone, A. Greco, M. Puopolo, G. Levi, A. J. Green, R. Knight and M. Pocchiari
765 (2002). "Increased CSF levels of prostaglandin E(2) in variant Creutzfeldt-Jakob disease."
766 Neurology **58**(1): 127-129.
767 Minghetti, L., A. Greco, F. Cardone, M. Puopolo, A. Ladogana, S. Almonti, C. Cunningham, V.
768 H. Perry, M. Pocchiari and G. Levi (2000). "Increased brain synthesis of prostaglandin E2 and
769 F2-isoprostane in human and experimental transmissible spongiform encephalopathies." J
770 Neuropathol Exp Neurol **59**(10): 866-871.
771 Minikel, E. V., H. T. Zhao, J. Le, J. O'Moore, R. Pitstick, S. Graffam, G. A. Carlson, M. P.
772 Kavanaugh, J. Kriz, J. B. Kim, J. Ma, H. Wille, J. Aiken, D. McKenzie, K. Doh-Ura, M. Beck, R.
773 O'Keefe, J. Stathopoulos, T. Caron, S. L. Schreiber, J. B. Carroll, H. B. Kordasiewicz, D. E. Cabin
774 and S. M. Vallabh (2020). "Prion protein lowering is a disease-modifying therapy across prion
775 disease stages, strains and endpoints." Nucleic Acids Res **48**(19): 10615-10631.
776 Nakano, M., Y. Tamura, M. Yamato, S. Kume, A. Eguchi, K. Takata, Y. Watanabe and Y. Kataoka
777 (2017). "NG2 glial cells regulate neuroimmunological responses to maintain neuronal function
778 and survival." Sci Rep **7**: 42041.
779 Pandey, S., K. Shen, S. H. Lee, Y. A. Shen, Y. Wang, M. Otero-Garcia, N. Kotova, S. T. Vito, B. I.
780 Laufer, D. F. Newton, M. G. Rezzonico, J. E. Hanson, J. S. Kaminker, C. J. Bohlen, T. J. Yuen and
781 B. A. Friedman (2022). "Disease-associated oligodendrocyte responses across
782 neurodegenerative diseases." Cell Rep **40**(8): 111189.
783 Slota, J. A., B. V. Sajesh, K. F. Frost, S. J. Medina and S. A. Booth (2022). "Dysregulation of
784 neuroprotective astrocytes, a spectrum of microglial activation states, and altered
785 hippocampal neurogenesis are revealed by single-cell RNA sequencing in prion disease." Acta
786 Neuropathol Commun **10**(1): 161.
787 Sorce, S., M. Nuvolone, G. Russo, A. Chincisan, D. Heinzer, M. Avar, M. Pfammatter, P.
788 Schwarz, M. Delic, M. Muller, S. Hornemann, D. Sanoudou, C. Scheckel and A. Aguzzi (2020).
789 "Genome-wide transcriptomics identifies an early preclinical signature of prion infection."
790 PLoS Pathog **16**(6): e1008653.
791 Stuart, T., A. Butler, P. Hoffman, C. Hafemeister, E. Papalexi, W. M. Mauck, 3rd, Y. Hao, M.
792 Stoeckius, P. Smibert and R. Satija (2019). "Comprehensive Integration of Single-Cell Data."
793 Cell **177**(7): 1888-1902 e1821.
794 Wareham, L. K., S. A. Liddelow, S. Temple, L. I. Benowitz, A. Di Polo, C. Wellington, J. L.
795 Goldberg, Z. He, X. Duan, G. Bu, A. A. Davis, K. Shekhar, A. Torre, D. C. Chan, M. V. Canto-Soler,
796 J. G. Flanagan, P. Subramanian, S. Rossi, T. Brunner, D. E. Bovenkamp and D. J. Calkins (2022).
797 "Solving neurodegeneration: common mechanisms and strategies for new treatments." Mol
798 Neurodegener **17**(1): 23.
799 Wolock, S. L., R. Lopez and A. M. Klein (2019). "Scrublet: Computational Identification of Cell
800 Doublets in Single-Cell Transcriptomic Data." Cell Syst **8**(4): 281-291 e289.

801 Woodling, N. S., Q. Wang, P. G. Priyam, P. Larkin, J. Shi, J. U. Johansson, I. Zagol-Ikapitte, O.
802 Boutaud and K. I. Andreasson (2014). "Suppression of Alzheimer-associated inflammation by
803 microglial prostaglandin-E2 EP4 receptor signaling." J Neurosci **34**(17): 5882-5894.
804 Yang, S., S. E. Corbett, Y. Koga, Z. Wang, W. E. Johnson, M. Yajima and J. D. Campbell (2020).
805 "Decontamination of ambient RNA in single-cell RNA-seq with DecontX." Genome Biol **21**(1):
806 57.
807 Zhu, C., U. S. Herrmann, J. Falsig, I. Abakumova, M. Nuvolone, P. Schwarz, K. Frauenknecht, E.
808 J. Rushing and A. Aguzzi (2016). "A neuroprotective role for microglia in prion diseases." J Exp
809 Med **213**(6): 1047-1059.
810

811 **Figure legends**

812 **Figure 1**, NG2 glia activation in prion disease models. **a**-**b**, Western blots (**a**) and quantification
813 (**b**) of NG2 and NeuN in Tga20 COCS exposed to prions or non-infectious brain homogenates
814 (NBH, here and in subsequent figures). n = 6 samples/condition; 6-8 slices/sample. **c**-**d**, West-
815 ern blots (**c**) and quantification (**d**) of NG2 and Pdgfrα in brain tissues of mice inoculated with
816 prions or NBH. n = 6 mice/condition. **e**, NG2 immunofluorescence showing NG2 glia activation
817 in prion-infected Tga20 COCS vs Tga20 COCS exposed to NBH. Nuclei were stained with
818 DAPI (blue), here and henceforth. **f**, Quantification of NG2 immunointensity shown in **e**. n =
819 12 slices for NBH; n = 14 slices for Prion. **g**, NG2 glia activation in the cerebral cortex (Ctx),
820 hippocampus (Hip) and thalamus (Thal) of prion-inoculated mice vs mice inoculated with NBH.
821 **h**, Quantification of NG2 immunointensity shown in **g**. n = 6 mice/group. Here and in following
822 figures: *: $p < 0.05$; **: $p < 0.01$; ***: $p < 0.001$; n.s: not significant.
823

824 **Figure 2**, NG2 glia depletion enhances prion neurotoxicity and accelerates prion disease. **a**,
825 NeuN and NG2 immunofluorescence showing prion-induced neurodegeneration in NG2-glia-
826 depleted (CP673451) and NG2 glia intact (DMSO) Tga20 COCS. **b**, Quantification of NG2
827 immunointensity and NeuN positive area shown in **a**. n > 16 slices/condition. **c**, Survival curves
828 showing accelerated prion disease in NG2-glia-depleted (Pdgfrα^{iDTR}) mice after prion inocula-
829 tion. Median survival: 191 days for male Pdgfrα^{iDTR} mice; 205.5 days for male control mice;
830 174.5 days for female Pdgfrα^{iDTR} mice; 184 days for female control mice. NG2 glia depletion
831 was induced at 16 wpi. **d**, NG2 and Map2 immunofluorescence showing enhanced dendritic
832 pathology in hippocampi of NG2-glia-depleted (Pdgfrα^{iDTR}) mice after prion inoculation. Arrow-
833 heads: pathologic dendrites with varicosities and fragmentation. NG2 glia depletion was in-
834 duced at 16 wpi; brain samples were collected at 21 wpi. **e**, Quantification of NG2 im-
835 munointensity and Map2 positive area shown in **d**. n = 6 mice/group.
836

837 **Figure 3**, Loss of NG2 glia upregulates Cox2-Ptges expression. **a**-**b**, NG2 immunofluores-
838 cence (**a**) and quantification (**b**) in intact (DMSO) and NG2-glia-depleted (CP673451)
839 C57BL/6J COCS. n = 7 slices/condition. **c**, qRT-PCR results showing downregulation of NG2
840 and Pdgfrα and upregulation of Cox2 and Ptges in NG2-glia-depleted (CP673451) C57BL/6J
841 COCS. n = 6 samples; 6-8 slices/sample. **d**-**e**, NG2 immunofluorescence (**d**) and quantification
842 (**e**) in control (Ctrl) and PDGFAA-treated C57BL/6J COCS. n = 7 slices/condition. **f**, qRT-PCR
843 results showing upregulation of NG2 and Pdgfrα and downregulation of Cox2 and Ptges in
844 C57BL/6J COCS with increased NG2 glia density (PDGFAA) compared to NG2 glia intact
845 (Ctrl) C57BL/6J COCS. n = 6 samples; 6-8 slices/sample. **g**, qRT-PCR results showing up-
846 regulation of Cox2 and Ptges in NG2-glia-depleted (CP673451) Tga20 COCS after prion ex-
847 posure. n = 6 samples; 6-8 slices/sample. **h**, Cox2, Ptges and Iba1 immunofluorescence in

848 the hippocampus showing upregulation of Cox2 and Ptges and their colocalization with micro-
849 glia in brains of terminally sick prion-inoculated mice. **i**, Quantification of Cox2 and Ptges im-
850 munointensity shown in **h**. n = 3 mice for NBH and n = 4 mice for prion. **j**, Cox2 and Ptges
851 immunofluorescence in the hippocampus showing upregulation of Cox2 and Ptges in the
852 brains of NG2-glia-depleted (Pdgfrα^{iDTR}) mice compared to NG2 glia intact (Ctrl) mice after
853 prion inoculation. **k**, Quantification of Cox2 and Ptges immunointensity shown in **j**. n = 6
854 mice/group.
855
856 **Figure 4**, NG2 glia regulate microglial Cox2-Ptges through multiple mechanisms. **a**, UMAP of
857 single-cell RNA-seq data showing Cox2$^+$ and Ptges$^+$ microglia among total microglia in the
858 cerebral cortex of prion- or NBH-inoculated mice. **b**, Quantification of Cox2$^+$ and Ptges$^+$ mi-
859 croglia fractions against total microglia in the cerebral cortex of prion- or NBH-inoculated mice
860 shown in **a**. n = 4 mice for NBH and n = 8 mice for Prion. **c**, Venn diagram showing numbers
861 of shared and distinct DEGs of Cox2$^+$ and Ptges$^+$ microglia in the cerebral cortex of prion-
862 inoculated mice. **d**, Heatmap showing downregulation of homeostatic microglia signature
863 genes and upregulation of DAM and MHC$^+$ microglia signature genes as well as inflammatory
864 genes in Cox2$^+$ and Ptges$^+$ microglia in the cerebral cortex of prion-inoculated mice. **e**, Cell-
865 Chat analysis of cell-cell communications showing unaltered number of interactions (plotted
866 as the thickness of the edges) but reduced strength of interactions (plotted as the thickness of
867 the edges) from NG2 glia to Cox2$^+$ microglia in the cerebral cortex of prion-inoculated mice. **f**,
868 Heatmaps showing significantly weakened NG2 glia to Cox2$^+$ microglia interaction pathways
869 in the cerebral cortex of prion-inoculated mice. **g**, Immunofluorescence showing that NG2-
870 glia-derived factors such as Tgfb2, Pleiotrophin and Midkine but not Bmp7 and Semaphorin3d
871 suppress Ptges expression in primary microglia in the presence or absence of prions. **h**, Quan-
872 tification of Ptges immunointensity in microglia in the absence of prions shown in **g**. n = 4
873 independent experiments. **i**, Quantification of Ptges immunointensity in microglia in the pres-
874 ence of prions shown in **g**. n = 4 independent experiments.
875
876 **Figure 5**, Cox2-Ptges inhibition diminishes prion neurotoxicity and decelerates prion disease.
877 **a**-**b**, NeuN immunofluorescence (**a**) and quantification (**b**) showing enhanced neurodegener-
878 ation in PGE2-treated compared to DMSO-treated and PGD2-treated Tga20 COCS after prion
879 infection. n = 18 slices/condition. **c**-**d**, NeuN immunofluorescence (**c**) and quantification (**d**)
880 showing diminished neurodegeneration in Tga20 COCS treated with Ptges inhibitors C118
881 and C934 compared to DMSO-treated Tga20 COCS after prion infection. n = 18 slices/condi-
882 tion. **e**, Survival curves showing decelerated prion disease in Cox2 knockout (Cox2Luc) mice
883 compared to littermate WT mice. Median survival: 186 days for control mice; 199 days for
884 Cox2Luc mice. **f**-**g**, Map2 immunofluorescence (**f**) and quantification (**g**) showing diminished

885 dendritic pathology in the hippocampi of Cox2Luc mice after prion inoculation compared to
886 littermate WT mice. Brain samples were collected at 21 wpi. n = 6 mice/group.
887
888 **Figure 6,** Cox2-Ptges inhibition rescues enhanced neurodegeneration and accelerated prion
889 disease after NG2 glia depletion. **a**-**b**, NeuN immunofluorescence (**a**) and quantification (**b**)
890 showing that enhanced neurodegeneration in prion-infected, NG2-glia-depleted (CP673451)
891 Tga20 COCS can be rescued by treatment with Ptges inhibitors C118 and C934. n = 16
892 slices/condition. **c**, Cox2 ablation (Cox2Luc) suppresses the acceleration of prion disease in
893 NG2-glia-depleted (Pdgfrα^{iDTR}) mice. Median survival: 177 days for Pdgfrα^{iDTR}/WT mice; 184.5
894 days for Ctrl/WT mice; 199 days for Pdgfrα^{iDTR}/Cox2Luc and Ctrl/Cox2Luc mice. NG2 glia
895 depletion was induced at 16 wpi. **d**-**e**, Map2 immunofluorescence (**d**) and quantification (**e**)
896 showing enhanced dendritic pathology in NG2-glia-depleted (Pdgfrα^{iDTR}) hippocampi of prion-
897 infected mice, and its rescue by Cox2 ablation (Cox2Luc). n = 6 mice/group.
898
899 **Figure 7,** PGE2 enhances prion neurotoxicity mainly through the EP4 receptor (Ptger4)**. a**-**b**,
900 Live-cell imaging (**a**) and quantitative analysis (**b**) of chronically prion-infected HovS cells ex-
901 pressing control (Ctrl) transgene or one of the four PGE2 receptors (Ptger1-4). Effects of
902 PGE2 treatment on prion-induced cell toxicity were measured with the ratio of GFP signals
903 under the PGE2 condition against the DMSO condition. n = 4 independent experiments; 4
904 technical repeats/experiment. **c**, Immunofluorescence of NeuN, Map2 and Tau showing cel-
905 lular damages of prion-infected primary neurons treated with different concentrations of Ptger4
906 agonist L902688. **d**, Quantification of neuronal density as well as Map2 positive and Tau pos-
907 itive areas shown in **c**. n = 6 independent experiments. **e**-**f**, NeuN immunofluorescence (**e**)
908 and quantification (**f**) showing concentration-dependent enhancement of prion-induced neu-
909 rodegeneration in L902688-treated Tga20 COCS. n = 12 slices/condition.

Liu et al., Main figures

Figure 1

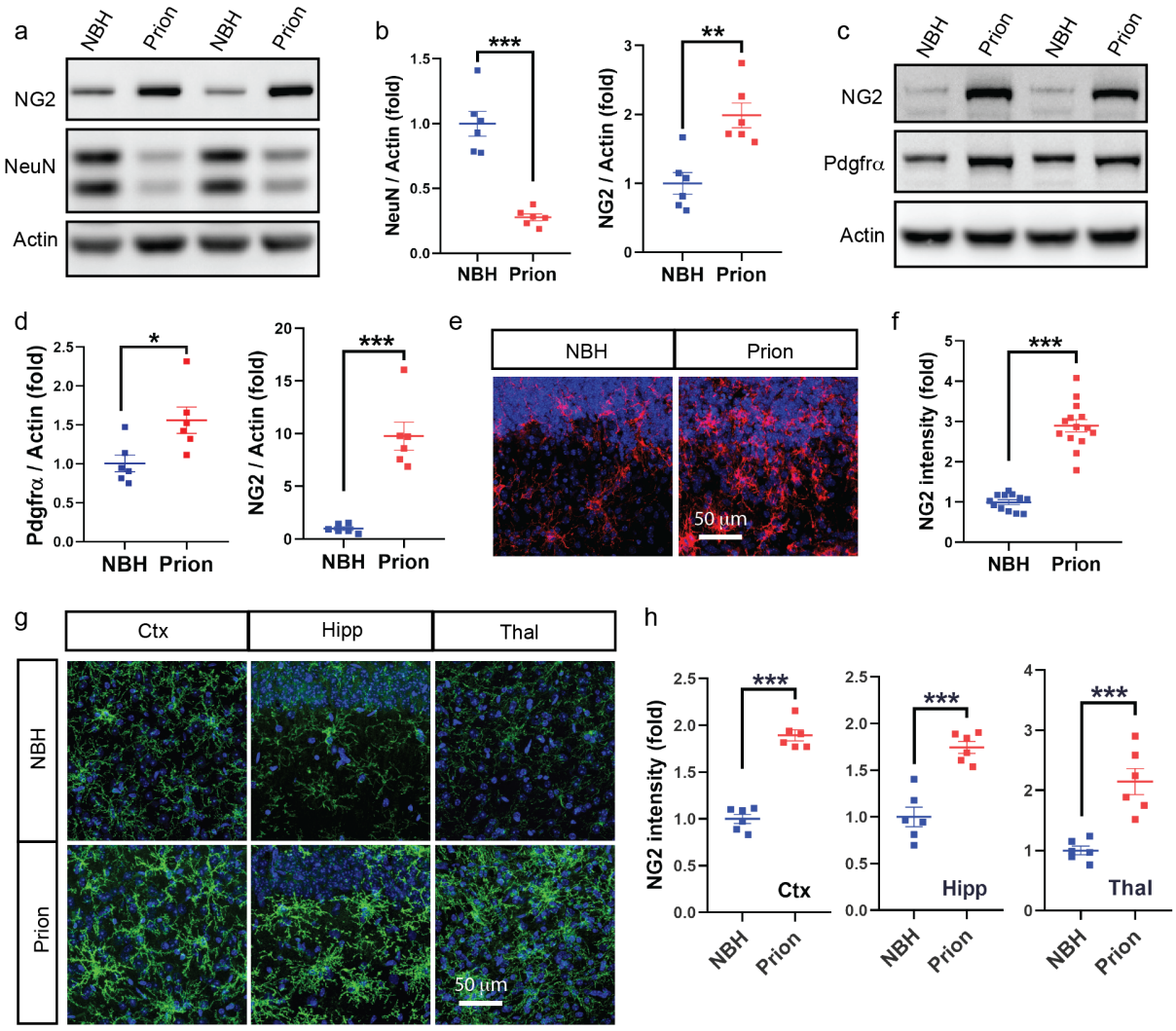

Figure 2

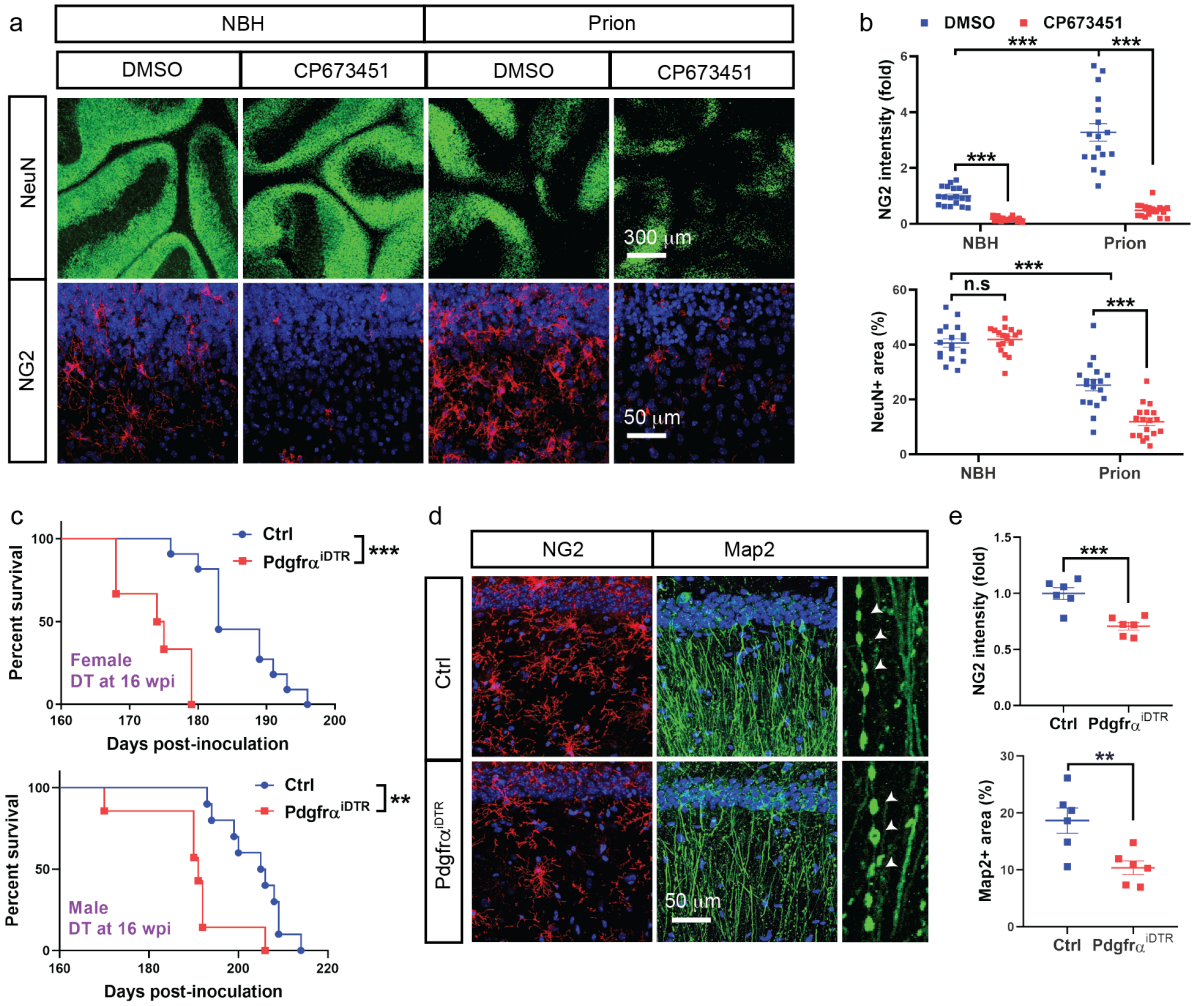
a
NBH
Prion
DMSO
CP673451
DMSO
CP673451
NeuN
NG2
300 μm
50 μm
b
DMSO
CP673451
NG2 intentsity (fold)
***
***
***
NBH
Prion
NeuN+ area (%)
n.s
***
***
NBH
Prion
c
Percent survival
Ctrl
Pdgfrα iDTR
***
Female
DT at 16 wpi
Days post-inoculation
Percent survival
Ctrl
Pdgfrα iDTR
**
Male
DT at 16 wpi
Days post-inoculation
d
NG2
Map2
Ctrl
Pdgfrα iDTR
50 μm
e
NG2 intensity (fold)
***
Ctrl
Pdgfrα iDTR
Map2+ area (%)
**
Ctrl
Pdgfrα iDTR

Figure 3

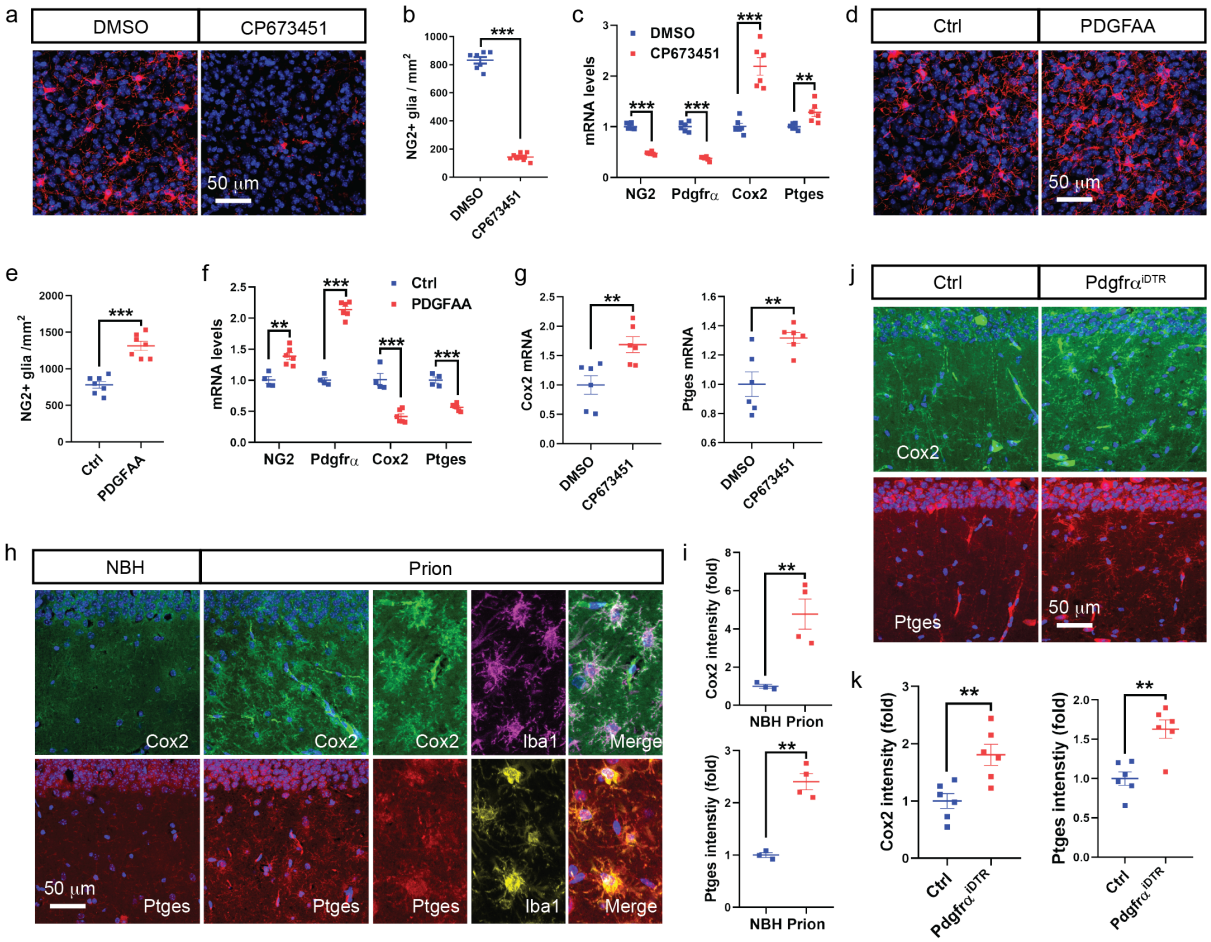
a
DMSO
CP673451
50 μm
b
NG2+ glia / mm2
DMSO
CP673451
c
DMSO
CP673451
mRNA levels
NG2
Pdgfrα
Cox2
Ptges
d
Ctrl
PDGFAA
50 μm
e
NG2+ glia /mm2
Ctrl
PDGFAA
f
Ctrl
PDGFAA
mRNA levels
NG2
Pdgfrα
Cox2
Ptges
g
Cox2 mRNA
Ptges mRNA
DMSO
CP673451
j
Ctrl
Pdgfrα iDTR
Cox2
Ptges
50 μm
h
NBH
Prion
Cox2
Iba1
Merge
Ptges
50 μm
i
Cox2 intensity (fold)
Ptges intensity (fold)
NBH Prion
k
Cox2 intensity (fold)
Ptges intensity (fold)
Ctrl
Pdgfrα iDTR

Figure 4

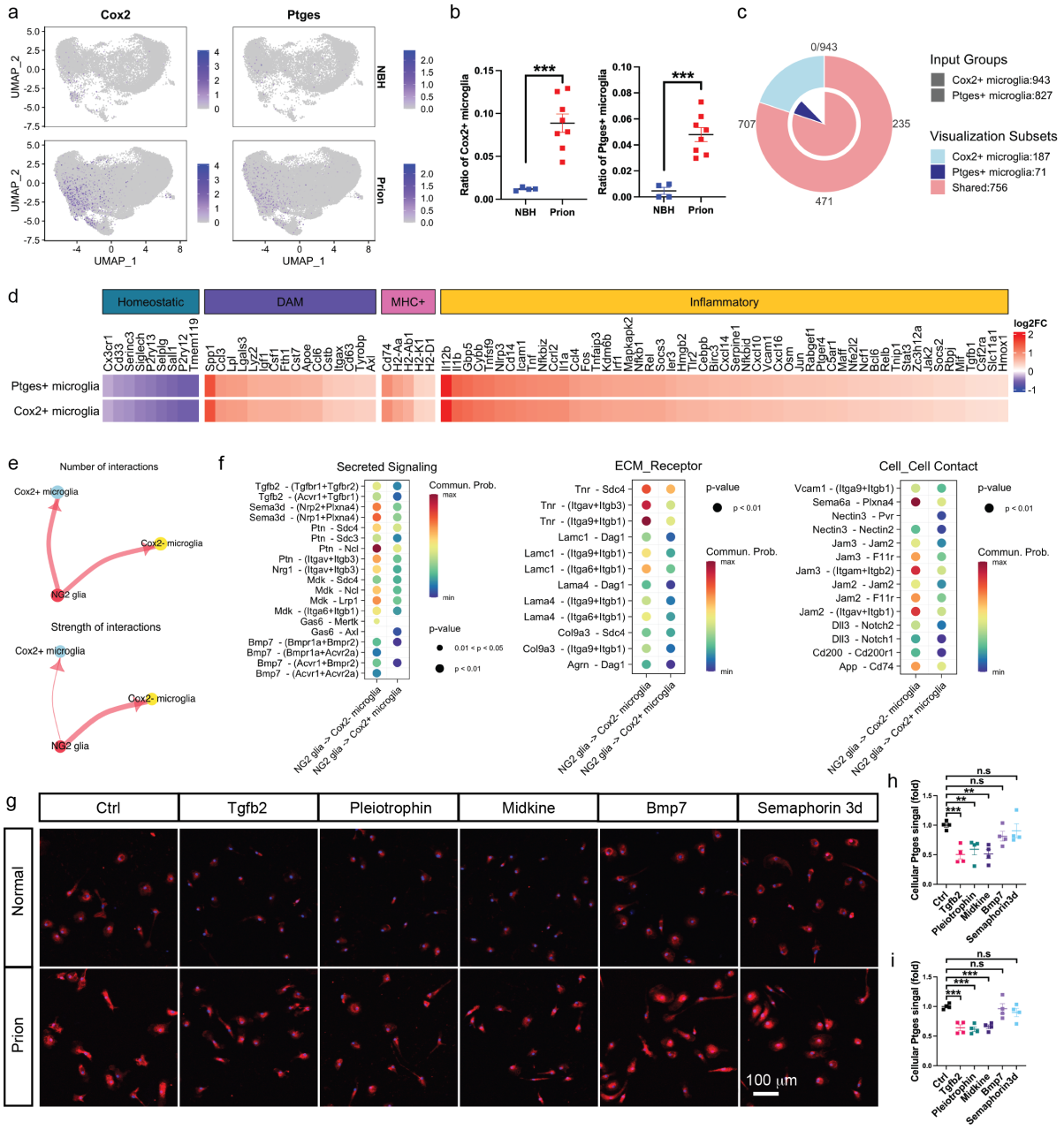
a
Cox2
Ptges
NBH
Prion
UMAP_1
UMAP_2
b
Ratio of Cox2+ microglia
Ratio of Ptges+ microglia
NBH
Prion
c
0/943
707
235
471
Input Groups
Cox2+ microglia:943
Ptges+ microglia:827
Visualization Subsets
Cox2+ microglia:187
Ptges+ microglia:71
Shared:756
d
Homeostatic
DAM
MHC+
Inflammatory
Ptges+ microglia
Cox2+ microglia
log2FC
e
Number of interactions
Cox2+ microglia
Cox2- microglia
NG2 glia
Strength of interactions
f
Secreted Signaling
ECM_Receptor
Cell_Cell Contact
Commun. Prob.
p-value
NG2 glia -> Cox2- microglia
NG2 glia -> Cox2+ microglia
g
Ctrl
Tgfb2
Pleiotrophin
Midkine
Bmp7
Semaphorin 3d
Normal
Prion
100 μm
h
i
Cellular Ptges singal (fold)
n.s

Figure 5

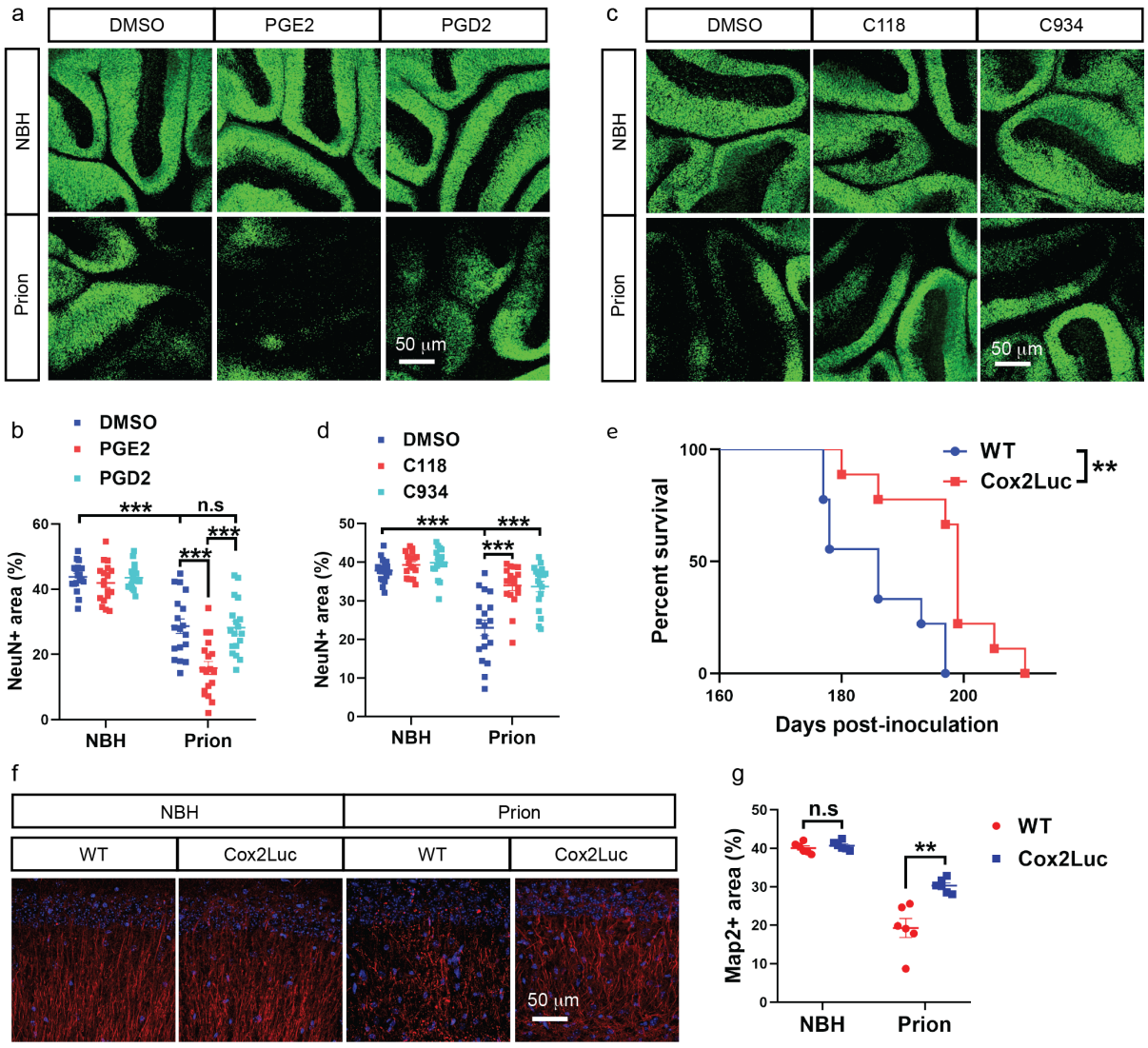
a
DMSO
PGE2
PGD2
NBH
Prion
50 µm
c
DMSO
C118
C934
NBH
Prion
50 µm
b
DMSO
PGE2
PGD2
NeuN+ area (%)
***
n.s
***
***
NBH
Prion
d
DMSO
C118
C934
NeuN+ area (%)
***
***
***
NBH
Prion
e
WT
Cox2Luc
**
Percent survival
Days post-inoculation
f
NBH
Prion
WT
Cox2Luc
WT
Cox2Luc
50 µm
g
Map2+ area (%)
n.s
**
WT
Cox2Luc
NBH
Prion

Figure 6

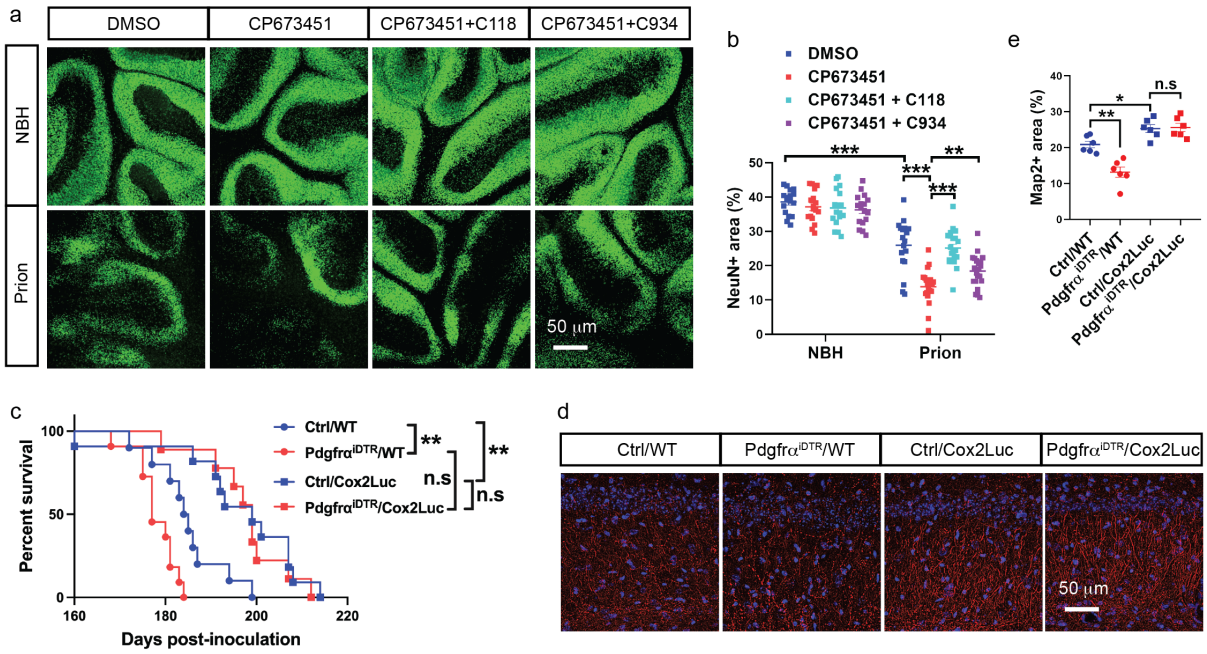
a
DMSO
CP673451
CP673451+C118
CP673451+C934
NBH
Prion
50 µm
b
DMSO
CP673451
CP673451 + C118
CP673451 + C934
NeuN+ area (%)
NBH
Prion
e
Map2+ area (%)
n.s
Ctrl/WT
PdgfrαiDTR/WT
Ctrl/Cox2Luc
PdgfrαiDTR/Cox2Luc
c
Percent survival
Days post-inoculation
Ctrl/WT
PdgfrαiDTR/WT
Ctrl/Cox2Luc
PdgfrαiDTR/Cox2Luc
n.s
d
Ctrl/WT
PdgfrαiDTR/WT
Ctrl/Cox2Luc
PdgfrαiDTR/Cox2Luc
50 µm

Figure 7

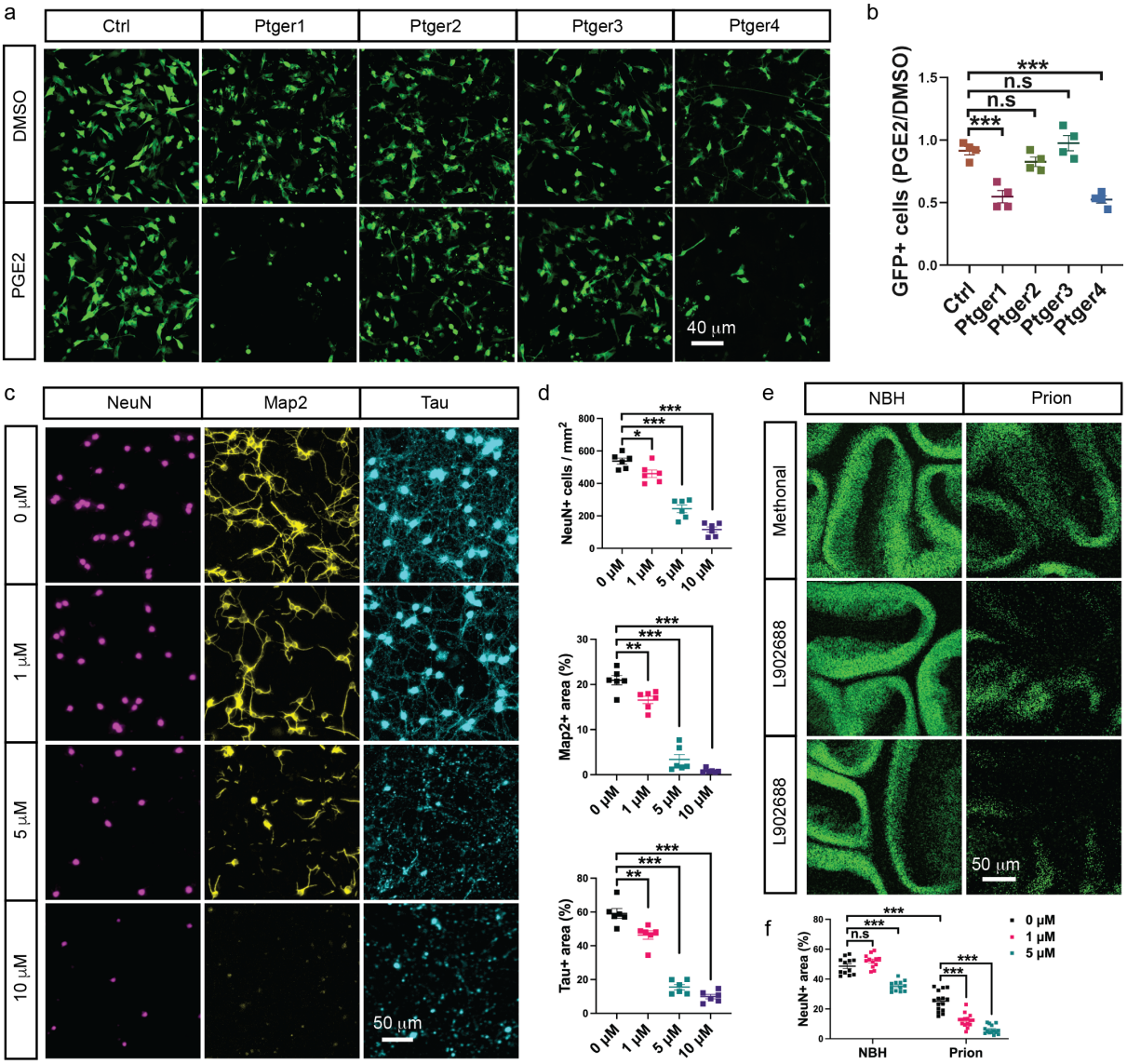
a
Ctrl
Ptger1
Ptger2
Ptger3
Ptger4
DMSO
PGE2
40 μm
b
GFP+ cells (PGE2/DMSO)
1.5
1.0
0.5
0.0
***
n.s
n.s
***
Ctrl
Ptger1
Ptger2
Ptger3
Ptger4
c
NeuN
Map2
Tau
0 μM
1 μM
5 μM
10 μM
50 μm
d
NeuN+ cells / mm2
800
600
400
200
0
Map2+ area (%)
30
20
10
0
Tau+ area (%)
80
60
40
20
0
0 μM
1 μM
5 μM
10 μM
e
NBH
Prion
Methonal
L902688
L902688
50 μm
f
NeuN+ area (%)
80
60
40
20
0
n.s
***
0 μM
1 μM
5 μM
NBH
Prion

Liu et al., Supplementary figures

Supplementary figure 1

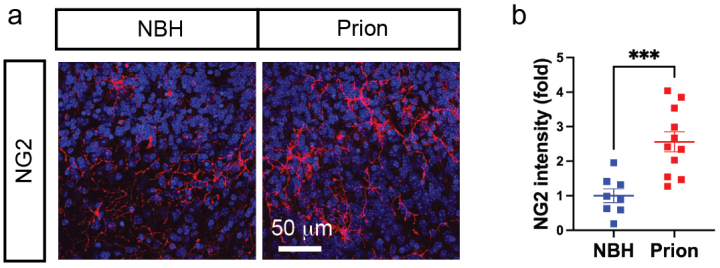

a, NG2 immunofluorescence showing NG2 glia activation in prion-infected C57BL/6J COCS vs C57BL/6J COCS exposed to NBH. Nuclei were stained with DAPI (blue). **b**, Quantification of NG2 immunointensity shown in **a**. n = 8 slices for NBH; n = 11 slices for Prion. Here and in following figures: *: $p < 0.05$; **: $p < 0.01$; ***: $p < 0.001$; n.s: not significant.

Supplementary figure 2

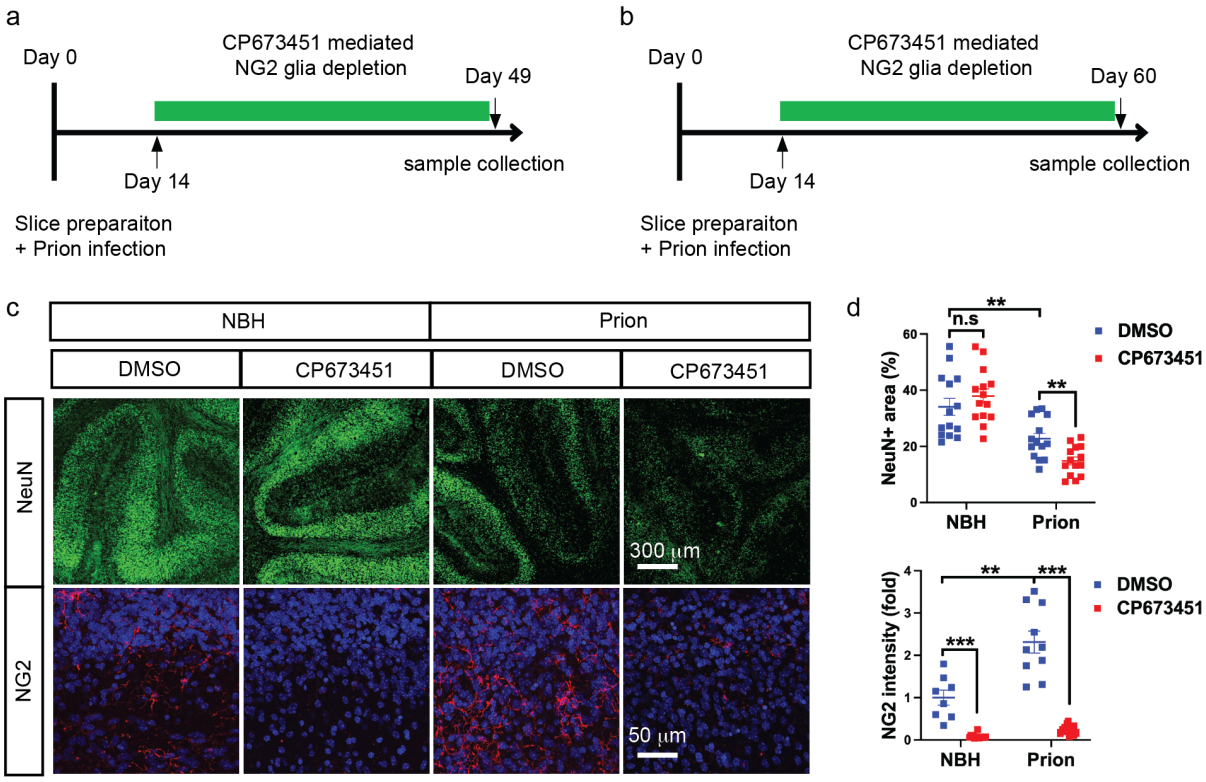

a-**b**, Experimental design of NG2 glia depletion in Tga20 COCS (**a**) and C57BL/6J COCS (**b**). **c**, NeuN and NG2 immunofluorescence showing enhanced neurodegeneration in continuously NG2-glia-depleted (CP673451) C57BL/6J COCS compared to NG2 glia intact (DMSO) C57BL/6J COCS after prion infection. Nuclei were stained with DAPI (blue). **d**, Quantification of NG2 immunointensity and NeuN positive area shown in **c**. n = 14 slices/condition for NeuN and n > 8 slices/condition for NG2.

Supplementary figure 3

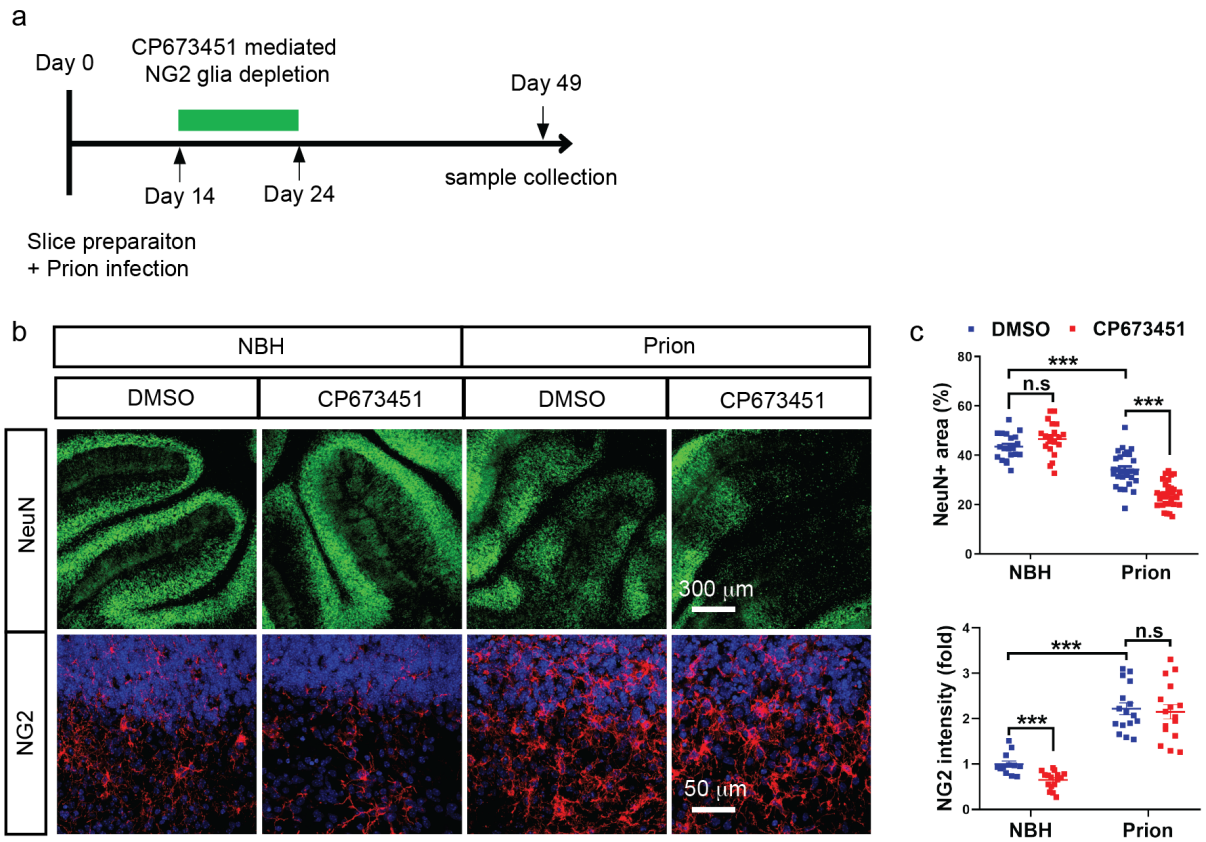

a, Experimental design of transient NG2 glia depletion in Tga20 COCS. **b**, NeuN and NG2 immunofluorescence showing enhanced neurodegeneration in transiently NG2-glia-depleted (CP673451) Tga20 COCS compared to NG2 glia intact (DMSO) Tga20 COCS after prion infection. NG2 glia density is largely recovered in prion-infected, transiently NG2-glia-depleted COCS at the end of the experiment. Nuclei were stained with DAPI (blue). **c**, Quantification of NG2 immunointensity and NeuN positive area shown in **b**. n > 16 slices/condition.

Supplementary figure 4

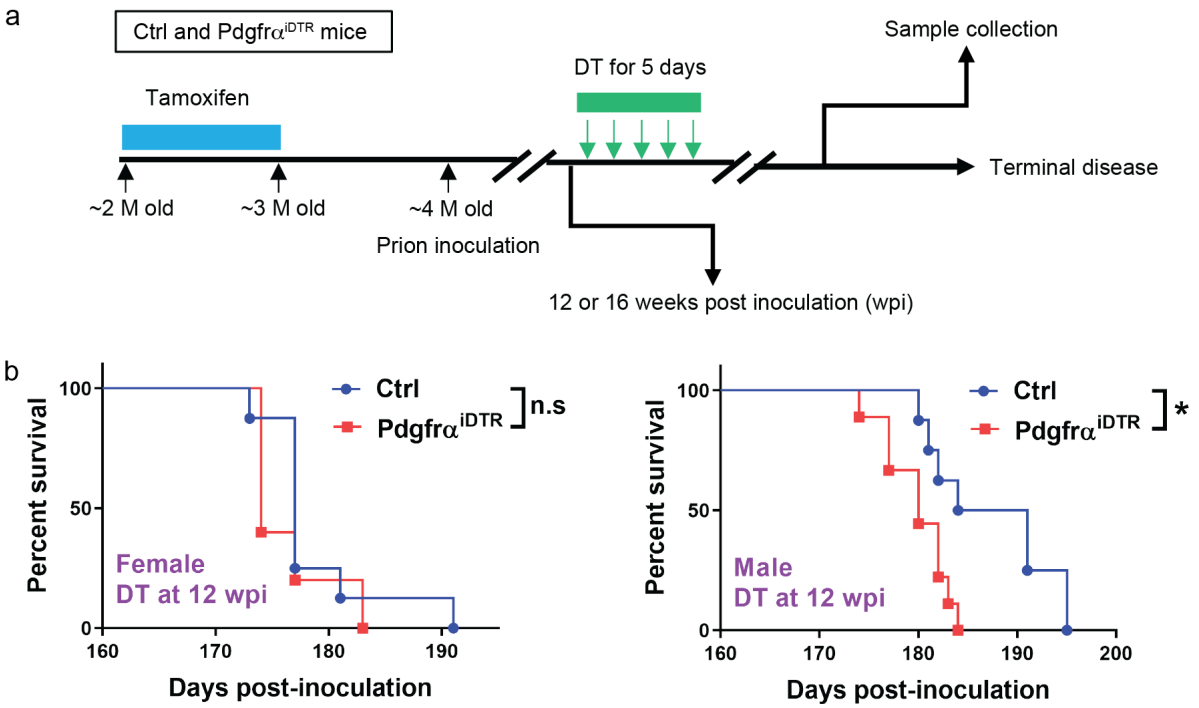

a, Experimental design of NG2 glia depletion in prion inoculated Pdgfrα^{iDTR} mice. Littermate Pdgfrα-CreER and iDTR mice were pooled together as control (Ctrl) and treated with tamoxifen and DT the same way as the Pdgfrα^{iDTR} mice. **b**, Survival curves showing accelerated prion disease in male, but not female NG2-glia-depleted (Pdgfrα^{iDTR}) mice compared to NG2 glia intact (Ctrl) mice after prion inoculation (median survival: 180 days for male Pdgfrα^{iDTR} mice; 187.5 days for male control mice; 174 days for female Pdgfrα^{iDTR} mice; 177 days for female control mice). NG2 glia depletion was induced at 12 wpi.

Supplementary figure 5

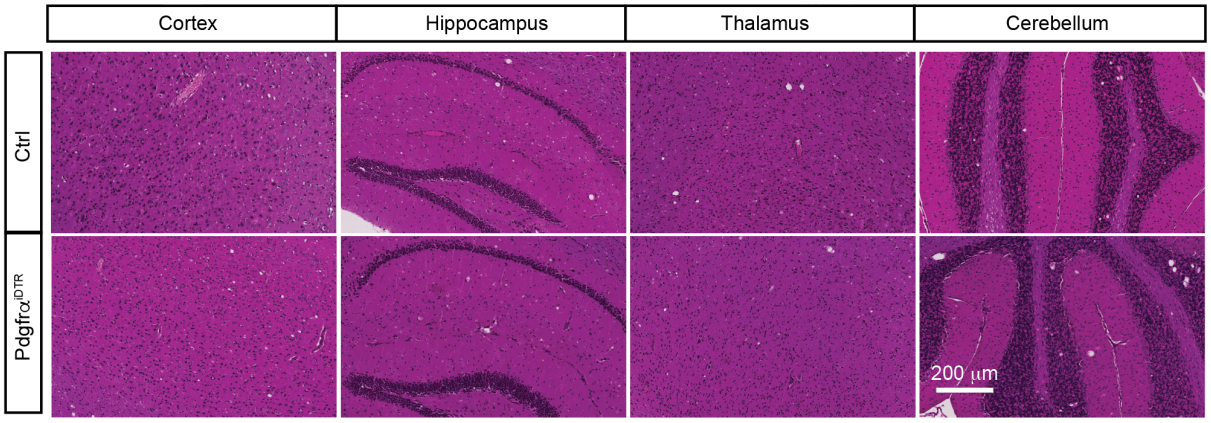

HE staining of brain tissues of NG2-glia-depleted (Pdgfrα^{iDTR}) and NG2 glia intact (Ctrl) mice after prion inoculation indicating similar vacuolation in different brain regions. NG2 glia depletion was induced at 16 wpi.

Supplementary figure 6

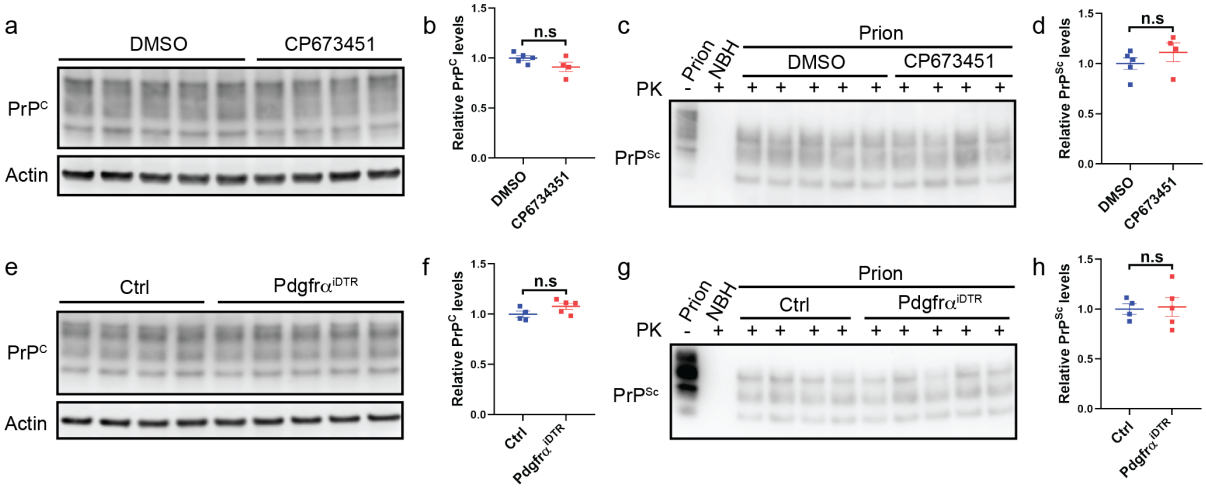

a-b, Western blots (**a**) and quantification (**b**) showing no changes of PrP^C level in NG2-glia-depleted (CP673451) Tga20 COCS compared to NG2 glia intact (DMSO) Tga20 COCS. n = 5 samples for DMSO and n = 4 samples for CP673451; 6 to 8 slices/sample. **c-d**, Western blots (**c**) and quantification (**d**) showing no changes of PK-resistant PrP^{Sc} levels in NG2-glia-depleted (CP673451) Tga20 COCS compared to NG2 glia intact (DMSO) Tga20 COCS after prion infection. n = 5 samples for DMSO and n = 4 samples for CP673451; 6 to 8 slices/sample. **e-f**, Western blots (**e**) and quantification (**f**) showing no changes of PrP^C levels in the brains of NG2-glia-depleted ($Pdgfr\alpha^{iDTR}$) mice compared to NG2 glia intact (Ctrl) mice. n = 4 mice for Ctrl and n = 5 mice for $Pdgfr\alpha^{iDTR}$. **g-h**, Western blots (**g**) and quantification (**h**) showing no changes of PK-resistant PrP^{Sc} levels in the brains of NG2-glia-depleted ($Pdgfr\alpha^{iDTR}$) mice compared to NG2 glia intact (Ctrl) mice after prion infection. NG2 glia depletion was induced at 16 wpi. n = 4 mice for Ctrl and n = 5 mice for $Pdgfr\alpha^{iDTR}$.

Supplementary figure 7

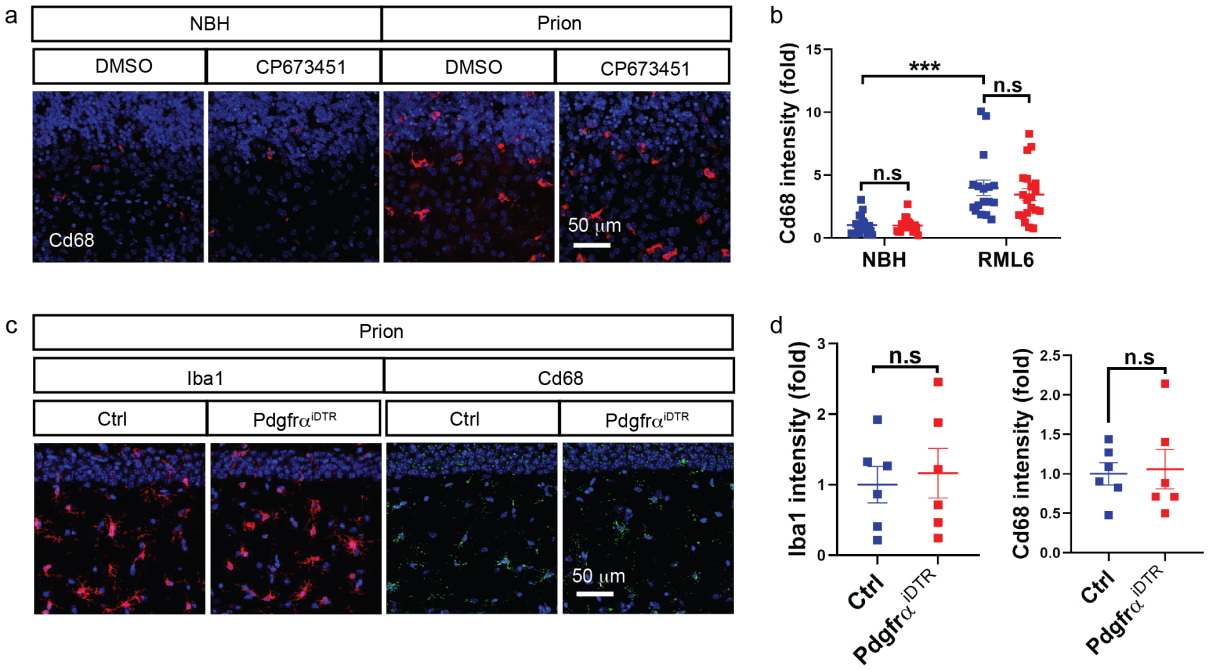

a-b, Cd68 immunofluorescence (**a**) and quantification (**b**) showing similar levels of microglia activation in NG2-glia-depleted (CP673451) Tga20 COCS compared to NG2 glia intact (DMSO) Tga20 COCS after prion infection. Nuclei were stained with DAPI (blue). n > 16 slices/condition. **c-d**, Iba1 and Cd68 immunofluorescence (**c**) and quantification (**d**) showing similar levels of microglia activation in the hippocampi of NG2-glia-depleted (Pdgfrα^{iDTR}) mice compared to NG2 glia intact (Ctrl) mice after prion infection. NG2 glia depletion was induced at 16 wpi. Nuclei were stained with DAPI (blue). n = 6 mice/group.

Supplementary figure 8

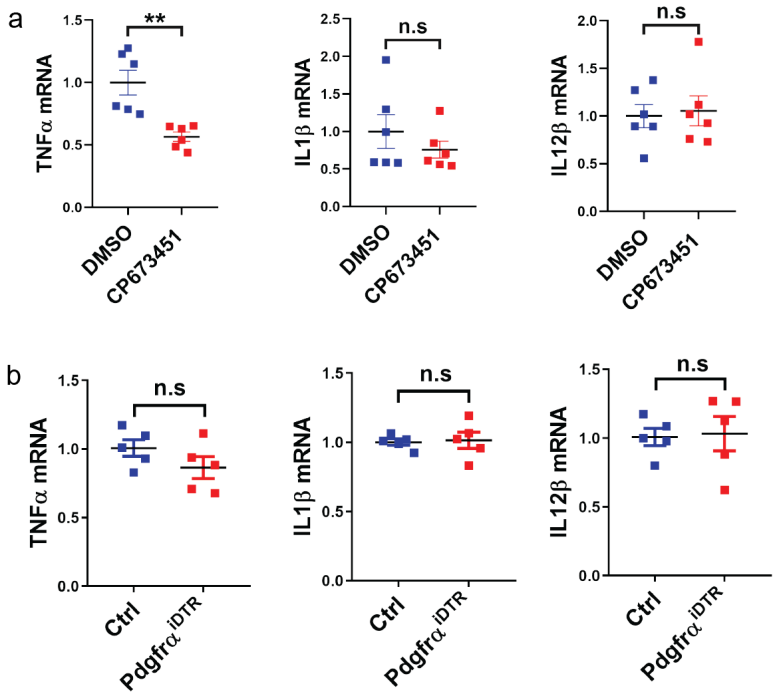

a, qRT-PCR results showing minimal changes of proinflammatory factors TNFα, IL1β and IL12β in NG2-glia-depleted (CP673451) Tga20 COCS compared to NG2 glia intact (DMSO) Tga20 COCS after prion infection. n = 6 samples/condition; 6 to 8 slices/sample. **b**, qRT-PCR results showing no changes of proinflammatory factors TNFα, IL1β and IL12β in the brains of NG2-glia-depleted (Pdgfrα^{iDTR}) mice compared to NG2 glia intact (Ctrl) mice after prion inoculation. n = 5 mice/group. NG2 glia depletion was induced at 16 wpi.

Supplementary figure 9

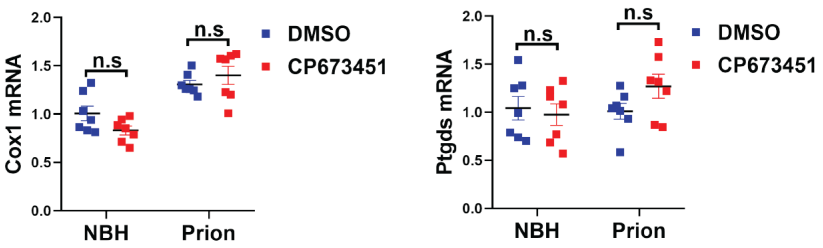

qRT-PCR results showing no changes of Cox1 and Ptgds in NG2-glia-depleted (CP673451) Tga20 COCS compared to NG2 glia intact (DMSO) Tga20 COCS in the presence or absence of prions. n = 7 samples/condition; 6 to 8 slices/sample.

Supplementary figure 10

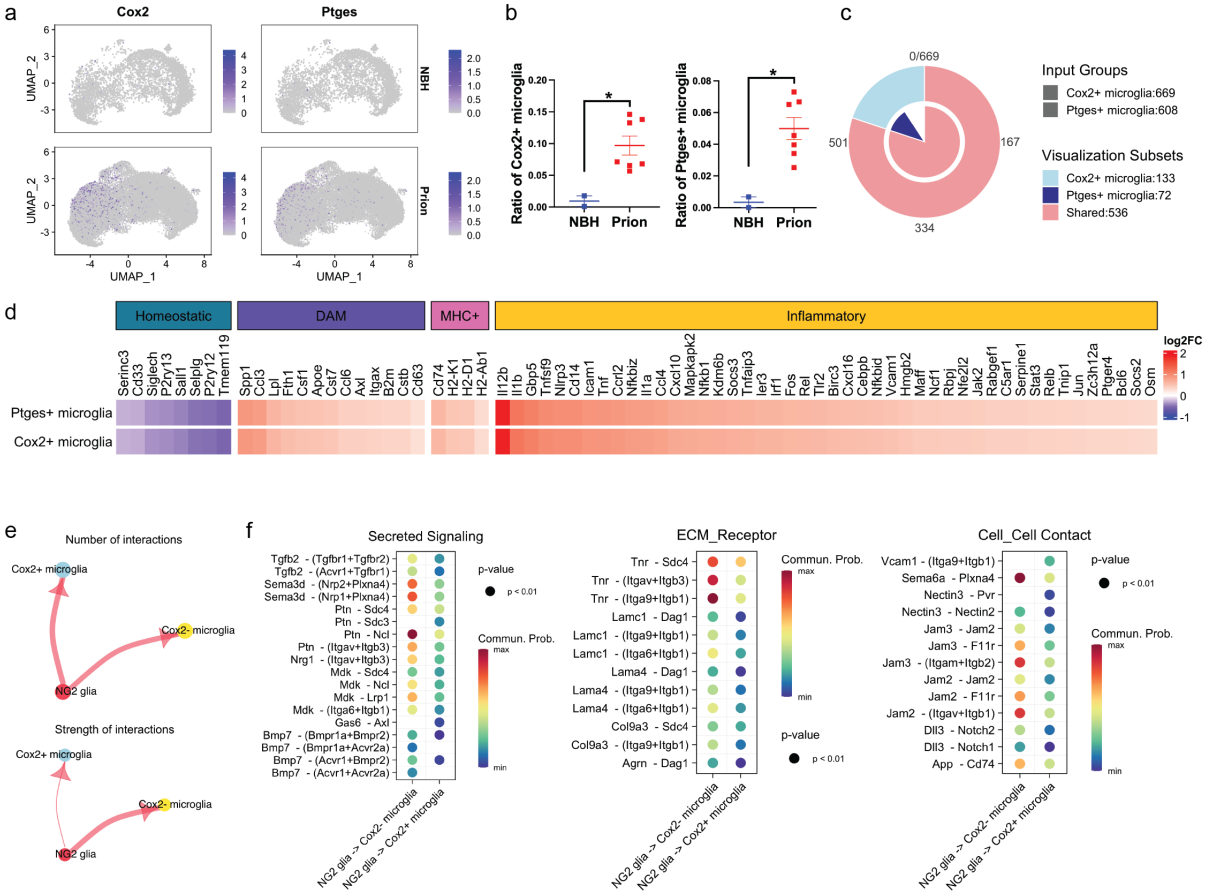

a, UMAP of single-cell RNA-seq data showing Cox2$^+$ and Ptges$^+$ microglia among total microglia in the hippocampus of prion- or NBH-inoculated mice. **b**, Quantification of Cox2$^+$ and Ptges$^+$ microglia fractions against total microglia in the hippocampus of prion- or NBH-inoculated mice shown in **a**. n = 2 mice for NBH and n = 7 mice for Prion. **c**, Venn diagram showing numbers of shared and distinct DEGs of Cox2$^+$ and Ptges$^+$ microglia in the hippocampus of prion-inoculated mice. **d**, Heatmap showing downregulation of homeostatic signature genes and upregulation of DAM and MHC$^+$ microglia signature genes as well as inflammatory genes in Cox2$^+$ and Ptges$^+$ microglia in the hippocampus of prion-inoculated mice. **e**, CellChat analysis of cell-cell communications showing unaltered number of interactions (plotted as the thickness of the edges) but reduced strength of interactions (plotted as the thickness of the edges) from NG2 glia to Cox2$^+$ microglia in the hippocampus of prion-inoculated mice. **f**, Heatmaps showing significantly weakened NG2 glia to Cox2$^+$ microglia interaction pathways in the hippocampus of prion-inoculated mice.

Supplementary figure 11

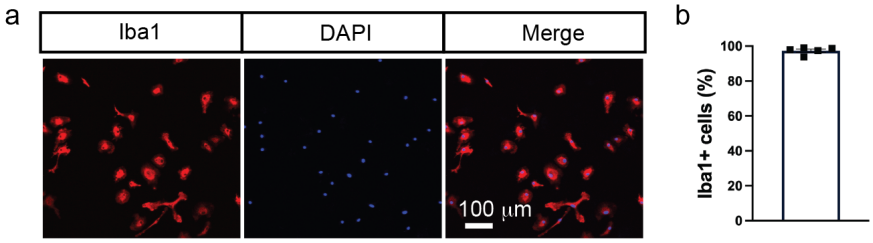

a, Iba1 immunofluorescence showing high purity of primary microglia cultures isolated by Cd11b immunopanning. Nuclei were stained with DAPI (blue). **b**, Quantification of Iba1+ cell percentage shown in **a**.

Supplementary figure 12

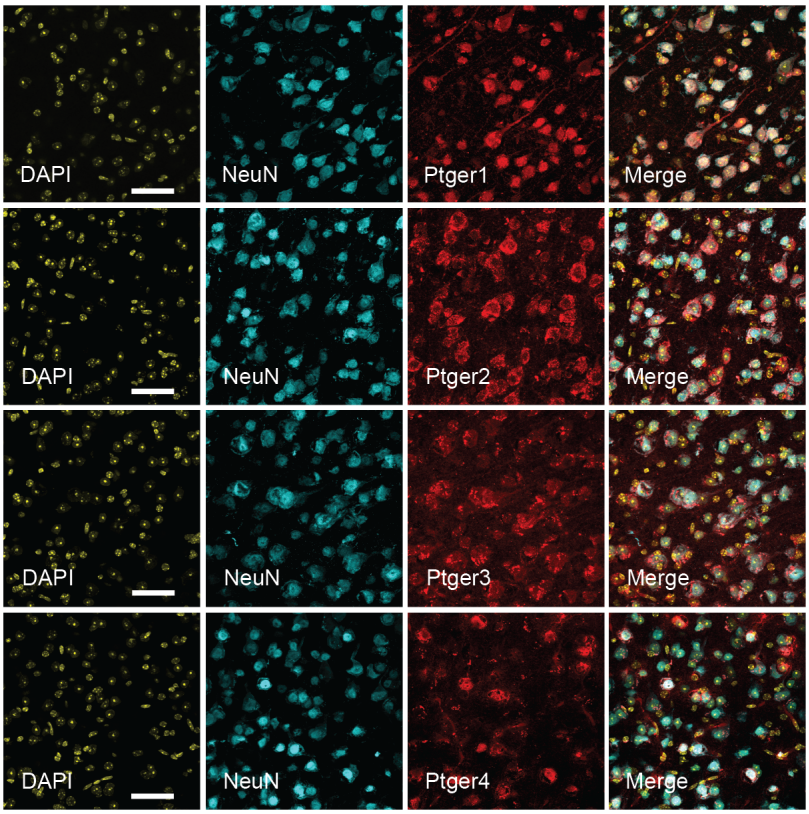

Immunofluorescence of NeuN and PGE2 receptors in the cerebral cortex showing neuronal expression of Ptger1, Ptger2, Ptger3 and Ptger4 in the adult mouse brain. Scale bar: 50 μm.

Supplementary figure 13

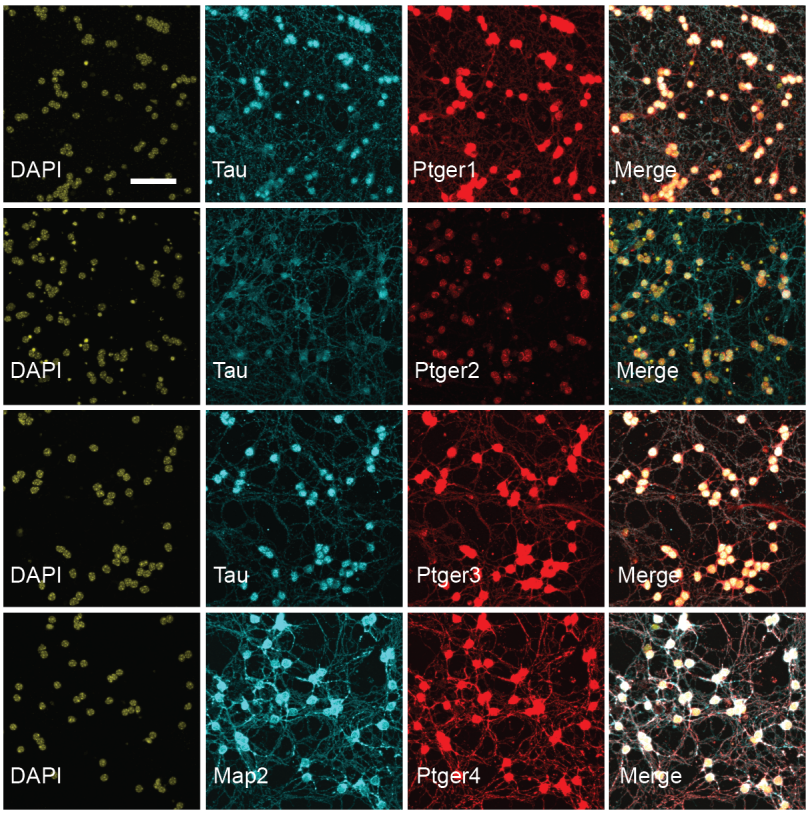

Immunofluorescence showing expression of Ptger1, Ptger2, Ptger3 and Ptger4 in the primary neuronal cultures (3 weeks in vitro). Ptger2 is mainly expressed in the neuronal cell body; Ptger1, Ptger3 and Ptger4 are expressed in both the neuronal cell body and neuronal processes. Scale bar: 50 μm.

Supplementary figure 14

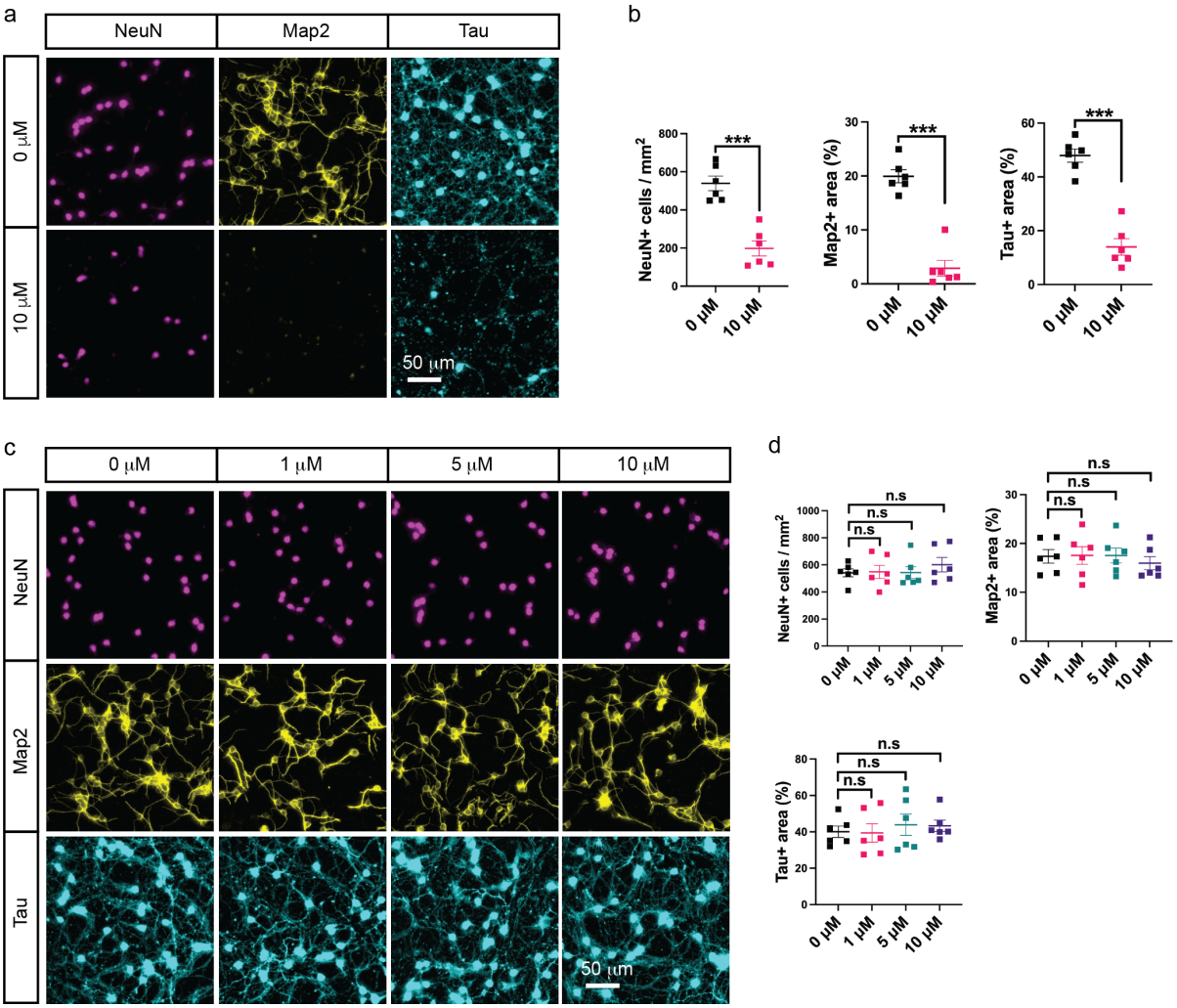

a, Immunofluorescence of NeuN, Map2 and Tau showing cellular damages of primary neurons treated with high concentration of Ptger4 agonist L902688. **b**, Quantification of neuronal density as well as Map2 positive and Tau positive areas shown in **a**. n = 6 independent experiments. **c**, Immunofluorescence of NeuN, Map2 and Tau showing no damages of prion-infected primary neurons treated with different concentrations of Ptger1 agonist 17-pt-PGE2. **d**, Quantification of neuronal density as well as Map2 positive and Tau positive areas shown in **c**. n = 6 independent experiments.

Supplementary figure 15

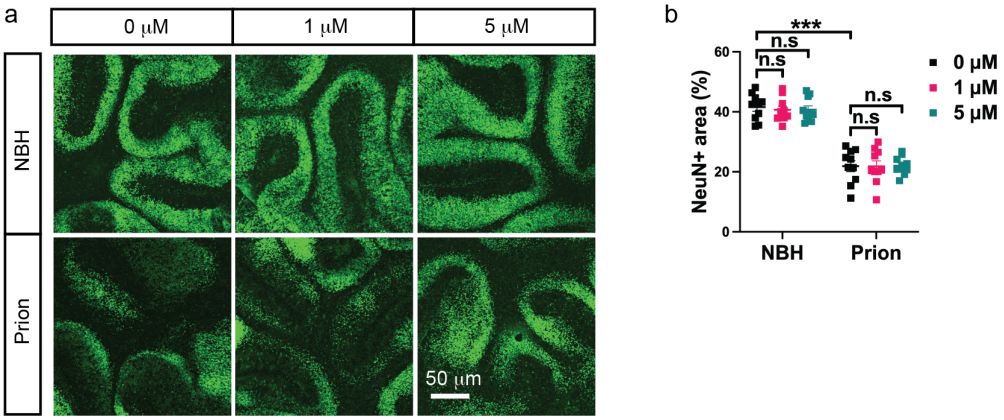

a-**b**, NeuN immunofluorescence (**a**) and quantification (**b**) showing no changes of prion-induced neurodegeneration in 17-pt-PGE2-treated COCS. n = 10 slices/condition.

Supplementary figure 16

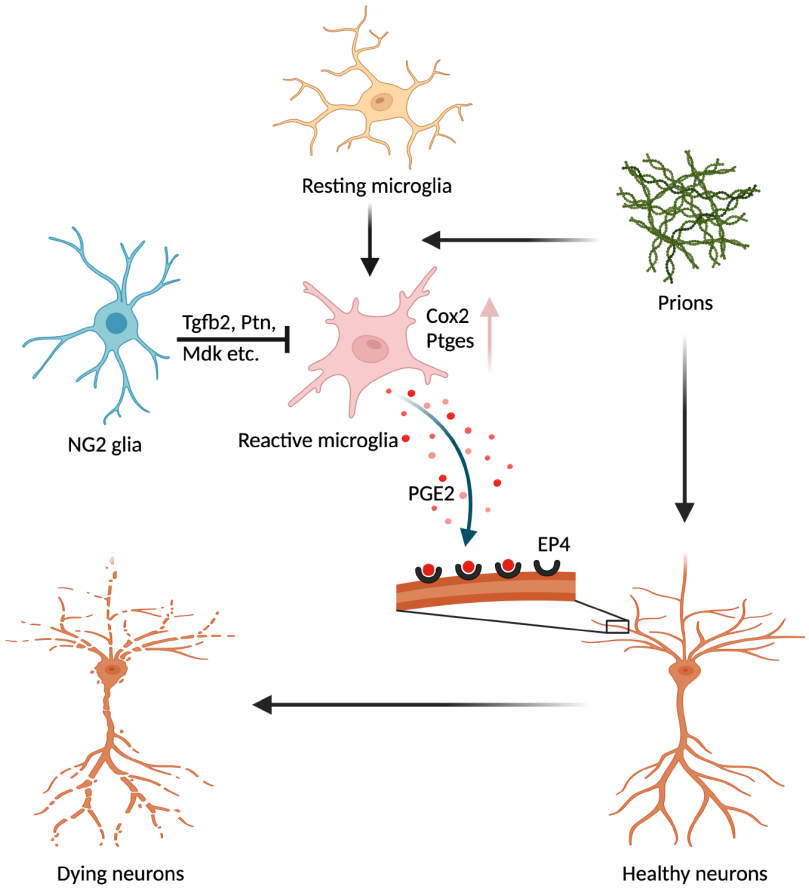

Diagram summarizing the main findings. In prion diseases, microglia become activated, and upregulate the pathway responsible for PGE2 biosynthesis, which promotes prion-induced neurodegeneration through binding to neuronal EP4 receptor. NG2 glia serve as a brake in this process, inhibiting microglial Cox2-Ptges pathway and PGE2 biosynthesis through multiple mechanisms (e.g., secreted signaling, ECM-receptor interaction and cell-cell contact). Several NG2-glia-derived factors playing a role in this process, such as Tgfb2, Pleiotrophin (Ptn) and Midkine (Mdk) are highlighted in the diagram.

Supplementary figure 17

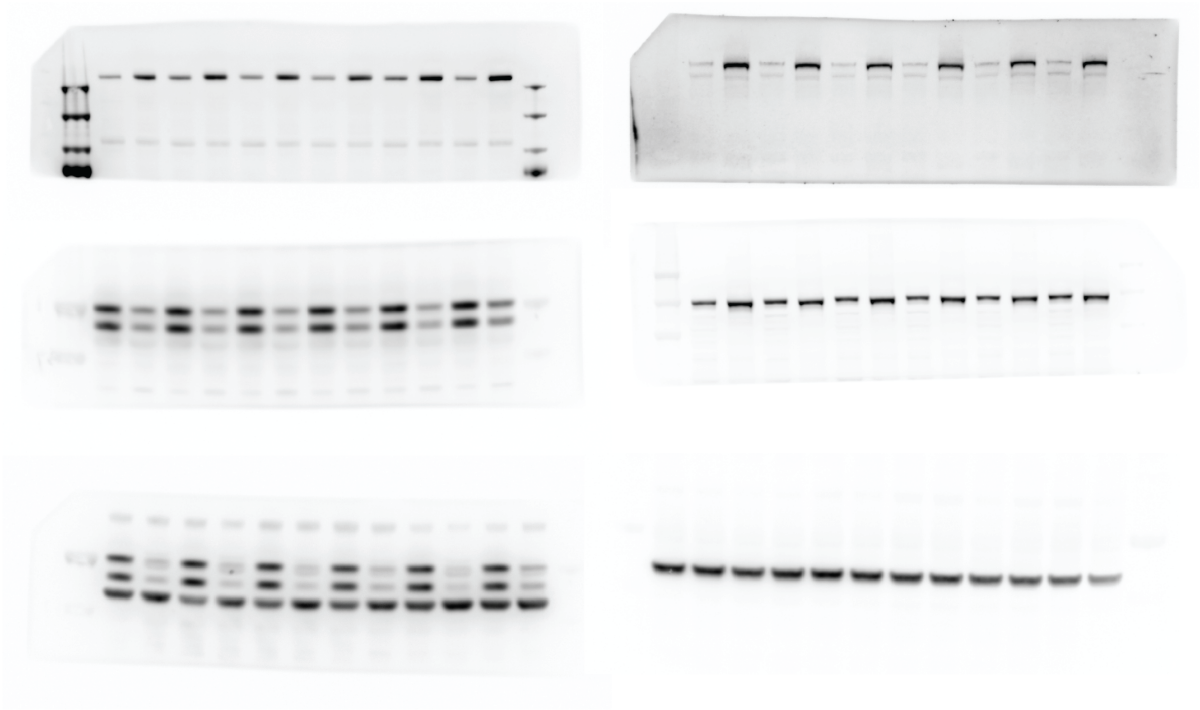

Uncropped western blots shown in figure 1.